Alginate microbead production for diabetes cellular therapy

Karen Markwick

Department of Chemical Engineering

McGill University, Montreal

Montreal, Quebec, Canada

December 2016

A thesis submitted to McGill University in partial fulfillment of the requirements for the degree of Masters of Engineering

Abstract

The predominant treatment for type 1 diabetes, insulin injections to regulate blood glucose levels, requires frequent blood glucose monitoring, injections, and is often associated with episodes of hypoglycaemia. Islet transplantation has emerged as an alternative cell-based therapy for type 1 diabetes to avoid the need for exogenous insulin. The Edmonton protocol, in which islet cells are isolated from a donor pancreas and transplanted into a type 1 diabetic undergoing immune suppression, can result in insulin independence in > 40 % of recipients three years post-transplantation. Islet encapsulation in alginate beads is being investigated as a means to provide an immunoprotective barrier between the graft and the host immune system in order to overcome the need for chronic immune suppression. Traditional nozzle-based encapsulation methods produce highly uniform alginate beads, but limit the viscosity of alginate that can be used for encapsulation. An alternative stirred emulsification and internal gelation encapsulation approach has high production rates and can produce beads from highly concentrated alginate, but a broad bead size distribution is obtained. The objective of this work was to develop microchannel emulsification as a method to produce highly uniform, concentrated alginate beads at production rates sufficient for clinical islet transplantation. A dual-flow chamber system was designed, consisting in a microchannel plate with oblong straight-through channels mounted between two flow channels. Alginate droplets form as the to-be-dispersed phase flows through the channels and contacts an acidified continuous oil phase that also triggers internal gelation. Significant process development involving modification of the flow rate, continuous phase liquid, emulsifier, microchannel dimensions and material, and operating procedure was required to facilitate droplet formation and achieve stable bead production. The current process can be used to produce 4 mL/min/channel of 0.5% to 2.5% alginate beads of approximately 3 mm in diameter, with a coefficient of variation of 9 %. Microchannel emulsification represents a promising method to

encapsulate cells in concentrated alginate beads that are highly uniform at high production rates. The alginate bead production process described in this work is a promising new method for cellular therapy and other applications in the food, drug, cosmetic and other industries.

Resumé

Le traitement le plus courant pour le diabète de type 1, soit l'injection d'insuline pour réguler la glycémie, est associé à des épisodes d'hypoglycémie et nécessite une surveillance rigoureuse de la glycémie. La transplantation d'îlots pancréatiques est une thérapie cellulaire qui a émergé comme traitement alternatif du diabète de type 1 afin d'éviter d'avoir recours à l'insuline exogène. Le protocole d'Edmonton est une méthode selon laquelle les îlots isolés du pancréas d'un donneur sont transplantés chez un patient diabétique de type 1 placé sous immunosuppression. Plus de 40% de récipiendaires peuvent demeurer insulino-indépendants trois ans après la transplantation. L'encapsulation des îlots est étudiée comme un moyen d'établir une barrière immunoprotectrice entre la greffe et le système immunitaire de l'hôte afin d'éviter d'avoir recours à l'immunosuppression. Habituellement, la production de billes d'alginate de taille uniforme est effectuée grâce à des procédés par buse, ce qui restreint la viscosité de la solution d'alginate qui peut être employée. Un procédé alternatif, l'émulsification en cuve agitée avec gélification interne, permet d'obtenir des taux de production plus élevés ainsi que l'utilisation de solutions d'alginate plus concentrées, mais cette méthode conduit à distribution de taille des billes très étendue. L'objectif de ce projet de recherche était de développer une méthode d'émulsification par microcanaux pour produire des capsules d'alginate très uniformes et concentrées, avec des taux de production adéquats pour la transplantation d'îlots chez les humains. Un système comportant deux chambres de flux séparées par une plaque traversée par des microcanaux oblongs a été conçu. Ce système permet la formation de gouttelettes d'alginate lorsque la phase dispersée traverse les canaux et entre en contact avec la phase hydrophobe continue. Le procédé a été

considérablement modifié en ajustant le débit, la composition de la phase liquide continue, l'émulsifiant, la dimension des microcanaux, les matériaux, ainsi que le mode d'opération requis afin d'améliorer la formation de gouttelettes et la production uniforme des billes. Le procédé actuel permet de produire des capsules d'alginate avec des concentrations entre 0,5% et 2,5% ayant un diamètre d'environ 3 mm et un coefficient de variation de 9% à un taux de 4 mL/min/canal. L'émulsification par microcanaux représente une méthode prometteuse pour encapsuler des cellules dans des capsules d'alginate uniformes à des taux de production élevés. Hormis la thérapie cellulaire, le procédé présenté peut être envisagé dans de nombreuses applications pour l'industrie alimentaire, pharmaceutique et cosmétique.

Acknowledgements

First, I would like to thank my supervisor, Dr. Corinne Hoesli, for her continued support and guidance. I could not have accomplished this work without your insight and recommendations. Thank you for taking me on as your first individually supervised graduate student; I feel honoured to be given the opportunity to see your lab grow into what it is today.

Thank you to all the members of the Hoesli lab, both past and present. The lab is truly a testament to everyone's efforts. Stephanie, you have been in the lab from the very start, and you have been so helpful to me, from offering ideas, advice, moral support, and a friendly ear. Natalie, thank you for your incredible help setting up the lab, making sure it ran smoothly, and offering moral support to myself and everyone in the lab. Marième and Ariane, thank you for your help with my French translations.

Thank you to Dr. Begin-Drolet and Marc-André Dussault for your collaboration on making the microchannel plate. Thank you to Amy Bolt for your work in the lab.

Ranjan, Frank, and Lou, thank you for all of your help setting up the lab, finding equipment, offering support and ideas, and keeping me safe.

Thank you, Avital, for your support and encouragement during my thesis writing.

Finally, thank you to Mum, Dad, Nicky, and Adrienne. Mum and Dad, I would not be where I am without your unconditional love and support. Nicky, I am so lucky to have you to give advice and talk to. Adrienne, thank you for being there through this all.

List of Figures

List of Tables

Nomenclature

Ca_d	Capillary number of the dispersed phase
Ca_d^{MC}	Microchannel dimension-adapted capillary number
Ca_d^{θ}	Wettability-adapted capillary number
d	Droplet diameter
d_d	Diameter of expanding dispersed phase
d_e	Needle diameter
d_{hole}	Diameter of the channel
F_B	Buoyancy force
F_γ	Interfacial tension force
g	Gravity
l	Characteristic length
l_c	Channel length
$U_{d,MC}$	Flow velocity of dispersed phase inside the channel.
v	Dispersed phase velocity
w_c	Channel width
We	Weber number
γ	Interfacial tension between continuous and dispersed phase
ΔP_{Lap}	Laplace pressure of the dispersed phase
$\Delta\rho$	Density difference
η_d	Viscosity of the dispersed phase
θ_d	Contact angle of the dispersed phase on the microchannel surface
ρ	Liquid density
σ	Surface tension
γ	Interfacial tension between continuous and dispersed phase increased

1.0 Introduction

Type 1 diabetes is an autoimmune disease in which the insulin-producing beta cells are destroyed by the body's immune system. In a healthy individual, beta cells in the pancreas produce insulin, a hormone that regulates the uptake of glucose from the bloodstream into cells. Without functioning beta cells, insulin is not produced; this leads to a build-up of glucose in the bloodstream (Figure 1). Insulin injection is a common treatment to maintain euglycemia in patients with type 1 diabetes. Diabetes therapy using exogenous insulin requires frequent blood glucose monitoring, injections, and patient compliance, and is associated with episodes of severe hypoglycemia [1]. Even with blood glucose regulation, type 1 diabetics are at risk of disease-related complications such as kidney failure, blindness, nerve damage, heart attack, and stroke.

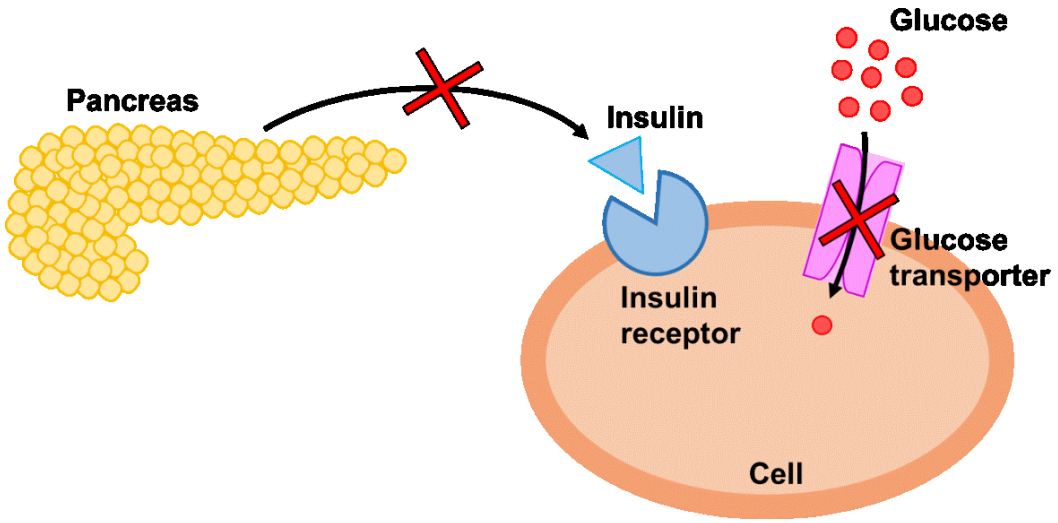

Figure 1. Process by which lack of insulin results in blood glucose build-up in type 1 diabetics.

There are currently over 300,000 Canadians and 1.25 million Americans living with type 1 diabetes [2, 3]. The incidence of type 1 diabetes is rising, with an expected increase of 3% annually in children under the age of 14 [3]. In addition, less than one third of type 1 diabetics in the USA achieve their target blood glucose levels [2]. An effective treatment for type 1 diabetes could dramatically increase the quality of life of millions of diabetics.

An alternative to insulin injections to regulate blood glucose levels is to provide an endogenous source of insulin, such as transplanted islet cells [4]. The Edmonton Protocol is a method of achieving insulin independence in humans through islet transplantation [5]. Islet cells are isolated from human donor pancreases and transplanted into patients undergoing an immunosuppression regimen. Islet transplantation can result in insulin independence for 3 years in >40% of patients [6]. The limited availability of donor islets poses a major hurdle to the use of transplanted islets as a therapy. However, with recent advances in stem cell and transplantation research, the use of pluripotent stem cells and xenogenic sources can be envisioned [7].

Another major limitation to islet transplantation is the need for lifelong immunosuppression [8]. Islet immunoisolation has been investigated for over 30 years as a means to avoid graft rejection without resorting to immunosuppressive drugs [9]. Immunoisolation is a bioengineering technique that consists of using a biocompatible material to create a permselective barrier between the graft and components of the host immune system, while allowing oxygen and nutrient transfer through the material [10]. Immunoisolation can be achieved through macroencapsulation or microencapsulation. Macroencapsulation involves many cells contained in a single immunoisolating device, while microencapsulation involves the distribution of the transplanted cells in many smaller capsules [10]. Oxygen limitation is thought to play an important role in the failure of encapsulated islet transplantation. Microbeads of < 1 mm in diameter offer increased diffusion capacity due to their higher surface to volume ratio [1]. Increasing the bead diameter reduces diffusive oxygen mass transfer rates to the islet [11], while decreasing the bead diameter increases the frequency of improperly encapsulated islets [12].

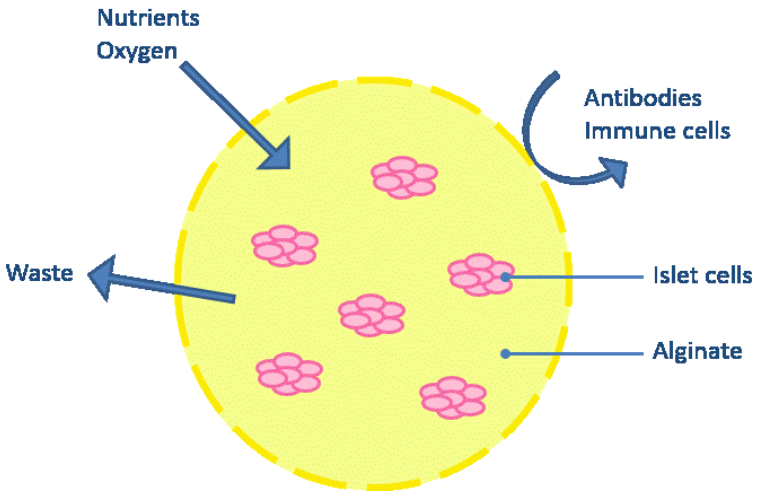

Figure 2. Microencapsulation immunoisolation

Pancreatic cells can be encapsulated in alginate, a water-soluble hydrogel that does not interfere with islet function and is stable in animals and humans [1]. Alginate forms a reversible ionotropic gel in the presence of divalent cations, such as calcium, at physiological pH and temperature [1]. A drawback to the use of alginate is large batch-to-batch variation. The composition of alginate varies greatly between different suppliers, and even between different batches from the same supplier [13]. As well, heat sterilization of alginate results in a significant decrease in the polymer chain length, hence molecular weight and viscosity [13]. A higher concentration of alginate leads to greater alginate chain entanglement, resulting in a higher viscosity [14]. The higher gel concentration will lead to a decreased pore size, decreased permeability to antibodies, and increased bead stability [15].

The alginate viscosity operating range, the bead production rate, and the bead size range of most commercially-available cell encapsulators are limited due to the need to form droplets at the tip of nozzles. This work proposes to use microchannel emulsification to produce highly uniform alginate beads for islet encapsulation, while allowing for the use of high-viscosity alginate solutions and achieving high production rates.

2.0 Literature Review

2.1 Encapsulation

Transplanting islet cells is a potential therapy for type 1 diabetes that could reduce or eliminate the need for chronic immunosuppression [10]. Encapsulated islet transplantation has been used to successfully treat type 1 diabetes in rodents. Long-term blood glucose normalization has been achieved after transplanting encapsulated syngeneic or allogenic islets in non-obese diabetic mice without immunosuppression [16-19]. Transplantation of pig islets into primates without immunosuppression showed partial islet survival and response to glucose challenge up to six months post-transplantation, with some fibrotic overgrowth [20, 21]. Transplantation of human islets into humans without immunosuppression has also been tested, showing a temporary decrease in the exogenous insulin needed [22]. Further investigation showed long-lasting detectable C-peptide expression, but no significant amounts of insulin [23]. Fibrotic overgrowth occurs when a matrix of fibroblasts and macrophages forms around the transplanted beads [24], and is a common problem resulting in decreased islet function and graft failure [23]. Increased levels of fibrotic overgrowth, an indication of the activation of the foreign body response, have been correlated with the presence of impurities in the encapsulation material, with islet protrusion from the beads, or with bead surface roughness [25].

2.1.1 Considerations for alginate bead production for islet encapsulation

A number of important considerations exist regarding the properties of alginate beads for islet encapsulation. Higher alginate concentrations (hence viscosities) decrease the bead pore size, thereby decreasing antibody permeability and increasing the bead stability [15]. The alginate viscosity has also been shown to affect the surface roughness, with higher viscosity alginate producing smoother beads [1]. Insufficient oxygen supply is also a common occurrence leading to decreased islet function. The encapsulated cells should have a diffusion length of no more than

~300 μm to avoid cell necrosis at the core of the islets [26-28]. Therefore, the alginate beads should be highly uniform in size. For islets encapsulated in 5% alginate beads at 2% islet packing density placed in an environment with venous (~60 mmHg) oxygen partial pressure, the optimal bead diameter was estimated to be ~ 600 μm [29]. Larger beads may limit oxygen diffusion to the cells, while smaller beads may result in improper encapsulation of the cells. Although islets are resilient to relatively high levels of energy dissipation rates [30], intense mechanical mixing or flowing viscous islet suspensions through small nozzles (in some cases smaller than the islet diameter) may damage the cells. Finally, a high production rate of the alginate beads is desirable. A transplant requires approximately one million islets [31]. If each bead contains on average one islet, ~100 mL of alginate beads would be needed to treat one patient. The encapsulation method should have the potential to produce the 100 mL required for one patient within a time frame that does not affect islet cell survival or function.

2.1.2 Nozzle-based Encapsulation Methods

The most common approach to encapsulate cells relies on droplet generation at the tip of a nozzle, followed by external gelation. In this approach, microscopic droplets formed by a nozzle-based encapsulator fall into a collection vessel containing a gelling solution such as calcium chloride [32]. This external gelation process relies on the diffusion of calcium or barium from the solution into the alginate droplets [33].

The simplest alginate droplet generation method relies on gravity for the formation of droplets. In this case, the droplets form when the droplet mass exceeds surface tension and viscous forces (Equation 1) [34]. This method produces large beads at a low production rate, and requires the use of alginate solutions with low viscosity (Table 1) [35]. Additionally, few studies have assessed the impact of the effect of the shear on the cells as they pass through the nozzle [30].

$$\boldsymbol{d} = \sqrt[3]{\frac{6d_e\sigma}{g\Delta\rho}} \qquad \textit{(Equation 1)}$$

Where d is the droplet diameter, d_e is the needle diameter, σ is the surface tension, and $\Delta\rho$ is difference between the liquid density and the air density.

Various methods can be employed to favour droplet formation at the tip of nozzles. Electrostatic encapsulators apply an electric charge to the fluid exiting the nozzle using a high voltage power source [34]. Pulsing the electric potential leads to the formation of uniform beads in a wide range of possible bead sizes. However, electrostatic encapsulation methods have limited scale-up potential, with production rates of approximately 5 mL/h for 300 µm beads [34], and the current methods limit the viscosity operating range (Table 1) [36].

An increased flow rate through the nozzle results in the formation of a jet, which can be broken into droplets using varying mechanical forces. Nozzle vibration [13, 34], a spinning disc [35], or a jet cutting tool [35] have all been used to produce droplets. The regimes of liquid jet breakup into droplets can be characterized according to the droplet sizes obtained. Droplets of a diameter similar to the nozzle diameter are obtained in the Rayleigh and the first wind-induced regime. In the Rayleigh regime, highly uniform droplets can be obtained when oscillations are superposed on a jet at a frequency that optimizes jet instability [37]. Multi-nozzle systems result in high production rates, but are currently limited to use with low viscosity fluids (Table 1) [38].

A spinning disc device can be used to form droplets several microns in size or larger; however, the droplets produced using this method have a large droplet size distribution and are limited to low viscosity fluids (Table 1) [35]. An additional problem associated with this method is the formation of satellite beads, which are significantly smaller than the average bead [39].

The JetCutter technology uses a rotating wheel with a fine wire to cut the extruding jet of liquid into droplets [35]. The JetCutter technology can produce monodisperse droplets from

200 μm to several millimeters in diameter with high viscosity fluids (Table 1), at flow rates of 2.1 – 4.1 L/h per nozzles for 600 μm beads [35]. However, bead production in aseptic conditions may be challenging using the JetCutter, and the shear stress applied during wire cutting may damage the cells [34]. Moreover, primary cell encapsulation has not yet been reported using this method.

2.1.3 Emulsion-based Encapsulation Methods

An emulsion and internal gelation approach to encapsulation has been developed as an alternative to the nozzle-based methods [31]. In this method, an emulsion is produced in a stirred vessel, forming droplets of alginate in oil. A mixture of alginate, cells, and calcium carbonate grains with low solubility at the initial process pH are added to mineral oil in a stirred vessel. After emulsification to generate microscopic droplets, an oil-soluble acid that preferentially partitions into the aqueous phase, such as acetic acid, is added to the vessel [31]. The decrease in pH triggers the release of Ca^{2+} from the calcium carbonate in the droplets, in turn gelling the alginate [40, 41]. Buffered saline solution is then added to the vessel, terminating the gelation by neutralizing the pH and triggering a phase inversion [31].

Emulsion and internal gelation offers a highly scalable alternative to the nozzle-based emulsification approach and can produce beads with diameters from 200 – 1000 μm [40]. The droplet breakup occurs due to the shear stress imparted on the viscous dispersed phase [31]. This approach can produce beads using a broad range of dispersed phase viscosities (Table 1).

Since the shear rate applied varies throughout the vessel with distance from the impeller tip, a broad bead size distribution is obtained by this method compared to nozzle-based encapsulators [31]. A narrow size range is preferable to achieve optimal diffusion kinetics while

avoiding islet protrusion from the beads [42]. There are also concerns regarding the effect of the shear stress imparted on the cells during droplet breakup.

2.1.4 Operating ranges of current mammalian cell encapsulation technologies

Table 1 (adapted from Hoesli, 2010 [43]) compares the various operating ranges of the previously described current mammalian cell encapsulation technologies.

Table 1. Operating ranges of current cell encapsulation technologies.

Process	Approximate maximum production rate (mL/h)	Range of alginate viscosities (Pa·s)	Bead diameter range (μm)	Tested *in vivo?*	Tested with pancreatic cells?
Emulsion & internal gelation [31, 44]	>30 000	0.004 – 112	250 – 1 500	✓	✓
Electrostatic bead generator [35, 45, 46]	100	0.03 – 11	300 – 5 000	✓	✓
Spinning disk [35, 47]	15 000	Not tested; 2 – 3 % alg.	Few hundred – several thousand		
Vibrating nozzle [35, 48, 49]	1 000	0.05 – 0.09	300 – 5 000	✓	✓
JetCutter [35, 50, 51]	1 000	0.15 – 11	200 – several thousand	✓	

2.2 Direct Droplet Emulsification

An emulsion can be produced using two methods. The first method is based on a mechanism whereby the dispersed phase continuously breaks up into smaller drops, such as in a stirred emulsification. The newly formed drops can coalesce when they come into contact with other drops; eventually, the droplet breakup rate matches the rate of coalescence, and the droplet size is stable with time. As the breakup and coalescence of the drops does not happen evenly throughout the stirred vessel, the resulting dispersed phase droplets vary in size. A second method, in which the final droplets are formed directly in one step, can produce more uniform dispersed

phase droplets. Membrane, microfluidic, and microchannel emulsification are all direct droplet production methods to produce an emulsion.

2.3 Membrane Emulsification

Membrane emulsification is a process to produce droplets by flowing a to-be-dispersed phase through a microporous membrane into a continuous phase, forming droplets directly at the membrane/continuous phase interface [52]. At low continuous phase flow rates, interfacial tension and steric hindrance between neighbouring droplets promote droplet detachment [53]. Above a critical continuous phase flow rate that depends on the device and pore geometry, the droplet detachment is promoted by shear stress from flow of the continuous phase, either by a cross flow pump [52] or stirring [54]. To increase droplet throughput, a centrifugal force can be exploited by utilizing a tubular membrane with the continuous phase being introduced radially [55]. Alternatively, the continuous phase can be static, with the shear stress being generated by a rotating [56] or vibrating [57] membrane.

The membranes are most commonly Shirasu Porous Glass or microsieve membranes. Shirasu Porous Glass membranes, the earliest emulsification membranes, have a uniform internal structure [58] and are commercially available with average pore sizes from 0.050 – 20 μm [53]. The resulting droplets usually have a diameter 3 ~ 4 times larger than the diameter of the pores with a relative span of 0.25 – 0.45 [59]. Production rates of 10 ~ 100 L m^{-2} h^{-1} can be achieved before continuous outflow of the dispersed phase occurs [60].

Microsieve membranes, which are increasingly common in membrane emulsification, have a controlled pore geometry and spatial arrangement. They can be produced using semiconductor fabrication methods [61] out of silicon nitride [62] or nickel [63], as well as laser drilling through

aluminium or stainless steel [64]. The droplets can have a diameter anywhere from 3 – 30 times larger than the diameter of the pore [65] and production rates up to 3200 L m^{-2} h^{-1} [66].

The droplet size is affected predominantly by the wetting properties of the membrane and membrane geometry, including pore size and spatial distribution [67]. The membrane must be hydrophobic to produce a water-in-oil emulsion and hydrophilic to produce an oil-in-water emulsion. Other parameters also play a role in droplet size, including the transmembrane pressure, wall shear stress, viscosity of the continuous and dispersed phase, and the surfactant type and concentration [67]. The droplet size decreases with increasing speed at which the surfactant molecules are transported to the newly forming continuous-dispersed phase interface. A minimum transmembrane pressure, known as the capillary pressure, is needed to drive the dispersed phase through the pores [67].

Membrane emulsification can be used to produce droplets from < 1 μm to several hundred μm, with a coefficient of variation from 10 – 20 % [67]. Given that islets are typically between 100 – 200 μm in size [68], the pore sizes of membrane emulsification devices are generally too small to accommodate islets. Membrane emulsification is likely to be problematic for use in islet encapsulation.

2.4 Microfluidic Emulsification

Microfluidic drop generation processes typically utilize planar channels, having at least one dimension smaller than 1 mm [69], to precisely produce droplets on a microscale. Microfluidic devices are most commonly microfluidic junctions and flow focusing devices. The devices are usually fabricated using a soft lithography process [69] to produce rectangular, open channels, most often in poly(dimethylsiloxane) [70]. The channels are then attached to a flat surface to

enclose them. Circular channels can also be created using stereolithography [71] or aligning and adhering two semicircle poly(dimethylsiloxane) channels [72], among other techniques.

T junctions are the simplest of the microfluidic devices [73]. The channel forms a T, in which the continuous phase flows through the main channel and the dispersed phase is introduced from a perpendicular channel. Shear stress and pressure upstream of the forming droplet cause elongation of the dispersed phase into the continuous phase channel until the dispersed phase neck pinches off and a droplet is formed in the main channel [74]. Three flow regimes exist in T junction droplet formation: squeezing, dripping, and jetting [75]. In the squeezing regime, the dispersed phase flows into almost the entire cross-section of the main channel at the junction as the shear stress exerted by the continuous phase is minimal. The continuous phase then occupies only a thin film around the channel walls, resulting in pressure build-up upstream of the junction [75]. Finally, the increased pressure causes the continuous phase to pinch the neck until droplet detachment occurs. In the squeezing regime, the droplet size is affected by the ratio of the two flow rates, while the interfacial tension or viscosity of the liquids have little impact [75]. In the dripping regime, the droplet detachment is promoted by the drag force that the continuous phase exerts on the emerging dispersed phase drop and is counteracted by the interfacial force. The size of the droplets is affected by the balance of these forces [75]. Above a continuous phase capillary number of 0.3, the droplet breakup occurs further downstream from the junction, eventually resulting in jetting of the dispersed phase [76].

Cross junction microfluidic devices have two continuous phase flows flanking the dispersed phase flow, pinching off droplets at the junction [77]. This technique applies Rayleigh's droplet formation approach [37] to microfluidics. Y junction devices represent another microfluidic mechanism, in which the continuous and dispersed phase flow in either branch,

mixing together in the main channel. Droplet formation is dependent on the continuous phase flow, with droplets forming above a critical Reynold's number. The size of the droplets is independent of the dispersed phase flow and viscosity [78]. Microfluidic flow focusing devices are similar to cross junctions with a small orifice that the combined two-phase flow is forced through [79]. The dispersed phase flows in the middle of three channels, with the continuous phase in the outer two channels. As the flows meet, the fluids are forced through an orifice. The dispersed phase flow is forced into a narrow thread due to the pressure and shear stress exerted by the continuous phase, resulting in breakup of the thread inside or downstream of the orifice.

Microfluidic devices can produce highly uniform droplets with coefficients of variation of < 3 %. However, the production rate of droplets per channel is very low [80]. The microfluidic channels can be multiplexed such that the inlet branches to an array up to thousands of channels, but this leads to a pressure drop along the channels. Moreover, the highest reported production rates of multiplexed microfluidic devices remain limited to ~300 mL/hour [81].

2.5 Microchannel Emulsification

Microchannel emulsification is a technique used to produce monodisperse oil-in-water and water-in-oil emulsions; the dispersed phase flows through microchannels, forming droplets into a continuous phase with tangential flow [82-84]. The droplets form due to the hydrodynamic instability of the dispersed phase stream exiting the channels. Microchannel emulsification can produce droplets from 1 μm in diameter [85] to several millimetres [86], with a coefficient of variation of less than 5% [84]. Microchannel emulsification employs a unique process called "spontaneous droplet generation" in which there is very low energy input and no external shear stress imparted on the droplets, resulting in a high degree of control over the droplet size [84, 87].

To promote droplet formation, the continuous phase must preferentially wet the surface of the microchannels [60]. For the production of an oil-in-water emulsion, a hydrophilic microchannel plate aids in droplet formation, while a hydrophobic plate is beneficial for the production of a water-in-oil emulsion. Silicon is commonly used as a substrate for microchannel plates, while hydrophobically-surface modified plates [88] or intrinsically hydrophobic poly(methyl methacrylate) plates can be used [89] for water-in-oil emulsions.

2.5.1 Straight-through microchannels

The microchannel configuration typically consists of either uniform, parallel microgrooves with a terrace [90, 91] or compactly arrayed, straight-through channels [92]. Grooved microchannels allow for experimental observation of the droplet generation as the movement of the oil-water interface can be clearly observed in the channels. It is difficult to see the movement inside straight-through microchannels. However, straight-through microchannels allow for higher droplet production, as they can accommodate over 100 times more microchannels per area than grooved microchannel arrays [90]. Straight-through microchannel arrays are scalable, with the potential of millions of microchannels in a single wafer [84]. They have been used to produce droplets at a dispersed phase flux of up to 1,200 $L \cdot m^{-2} \cdot h^{-1}$ [91], and dispersed phase viscosities of up to 50 mPa·s [93, 94].

Straight-through microchannels can be either symmetric [92] or asymmetric [95]. Asymmetric channels are of particular use when the dispersed phase viscosity is < 1 mPa s^{-1} [95], while symmetric channels can be used with higher dispersed phase fluxes and high dispersed phase viscosities [95]. The microchannel device is usually made of single-crystal silicon wafer with channels created by deep reactive ion etching.

For straight-through microchannels, oblong, rectangular channels increase the hydrodynamic instability of the dispersed phase as it contacts the continuous phase, leading to higher droplet formation rates and a minimized droplet/channel diameter ratio [96]. Oblong microchannels with a slot aspect ratio exceeding a threshold value of 3.5 have been shown to be optimal for producing monodisperse emulsions [97] with a coefficient of variation < 2 % [98] without mechanical stress [99]. Lower aspect ratios result in polydisperse droplets [100] or even jetting. Computational fluid dynamic simulations have been applied to oil-in-water systems that produce 40 μm droplets. These simulations show that aspect ratios of 3.5 or greater facilitate droplet formation in this context, whereas lower aspect ratios lead to continuous inflation of the dispersed phase from the channel exit [99]. Both the droplet diameter and droplet formation time decreased with an increase in channel aspect ratio from 3.5 to 3.75. No significant difference was observed when increasing the channel aspect ratio from 3.75 to 4.

Given a sufficient channel aspect ratio, the continuous phase flows into the exit of the channel and surrounds the channel wall, regardless of the flow of the continuous phase. Below this channel aspect ratio, increased continuous phase flow can promote the intrusion of the continuous phase at the exit of the channel and improve droplet formation to a point [99].

2.5.2 Forces affecting droplet formation

As the dispersed phase flows through the channel, the influx of the continuous phase aids in the formation of a neck just below the channel exit, which flows into the inflating droplet. The formation of this neck causes an increased pressure difference from the entrance to the exit of the neck, as well as an increased velocity in the neck. The pressure at the exit of the neck closely corresponds to the Laplace pressure of the dispersed phase, which can be calculated by the Young-Laplace equation (Equation 2) [99]:

$$\Delta \boldsymbol{P_{Lap}} = \frac{\boldsymbol{4\gamma}}{\boldsymbol{d}} \qquad \textit{(Equation 2)}$$

Where ΔP_{Lap} is the Laplace pressure of the dispersed phase, γ is the interfacial tensions, and d is the diameter of inflating dispersed phase.

The pressure difference between the neck and the inflating droplet promotes flow from the neck into the inflating droplet, which increases the pressure difference. Once the pressure difference has increased to a critical value, the flow from the neck into the inflating droplet exceeds the flow into the neck. The neck then shrinks until it is instantaneously cut off a result of the imbalance of outflow and inflow to the neck [99]. Once detached from the microchannel surface, the droplets spontaneously transform into spherical droplets with a diameter of approximately three times the channel width, or twice the hydraulic diameter [97, 100].

The droplet detachment occurs when the forces promoting droplet detachment outweigh the forces counteracting it. The buoyancy force (Equation 3) due to the density difference between the two phases promotes detachment, while the interfacial tension force (Equation 4) works to counteract it (Figure 3) [86]. Other forces, such as the inertial force, the drag force, and viscous forces [101], also act on droplet formation [86]. However, these forces are harder to characterize and manipulate in the microchannel emulsification process.

$$F_B = \left(\frac{\pi}{6}\right) {d_d}^3 g \Delta\rho \qquad \textit{(Equation 3)}$$

$$F_\gamma = \pi d_{hole} \gamma_{ow} \qquad \textit{(Equation 4)}$$

Where F_B is the buoyancy force, F_γ is the interfacial tension force, d_d is the diameter of the expanding dispersed phase, g is gravity, $\Delta\rho$ is the density difference between the continuous and dispersed phase, d_{hole} is the diameter of the channel, and γ_{ow} is the interfacial tension between the continuous and dispersed phase.

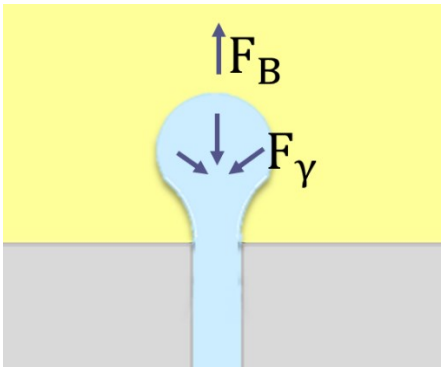

Figure 3. Balance of buoyancy and interfacial tension forces acting on droplet detachment.

Above the required microchannel aspect ratio, the size of the droplets generated is independent of the flow rate of the continuous phase up to a certain point [100]. Above the critical continuous phase flow rate, droplets will form due to the shear stress of the flowing continuous phase, similar to droplet formation in stirred emulsification of viscous dispersed phases. The effect of the dispersed phase flux on the droplet diameter depends on the droplet formation regime [60]. In the size-stable zone, below a critical dispersed phase flux value, uniform droplets are produced with diameters independent of the dispersed phase flux. In the continuous outflow zone, above a critical dispersed phase value, the droplets are dramatically larger and do not spontaneously detach; they only detach when they become large enough that the neighbouring droplets hinder their growth and force them to detach. Between these transition dispersed phase fluxes, in the size expanding zone, the droplets are irregularly sized and larger [102].

The capillary number of the dispersed phase represents the relative magnitude of the viscous and inertial forces [103]. It is useful in describing the dispersed phase flow transition in microchannel emulsification (Equation 5) [104]:

$$Ca_d = \frac{\eta_d U_{d,MC}}{\gamma_{eq}} \qquad \textit{(Equation 5)}$$

Where Ca_d is the capillary number of the dispersed phase, η_d is the viscosity of the dispersed phase, $U_{d,MC}$ is the flow velocity of the dispersed phase inside the channel, and γ_{eq} is the equilibrium interfacial tension.

For a given system, the dimensionless droplet diameter, the droplet diameter normalized to the diameter of the channel, is almost constant up to a critical capillary number. In this region, the interfacial tension force is dominant and there is spontaneous transformation of the dispersed phase into droplets at the exit of the channel. Above the critical capillary number, when the viscous forces are dominant, prolonged outflow of the dispersed phase is observed, resulting in prolonged droplet production, and increased droplet size. The critical capillary number is dependent on the operating temperature, viscosity, and microchannel dimensions [104]. The maximum production rate achievable increases with decreased dispersed phase viscosities [93].

A modified capillary number encompasses the effect of channel dimensions (Equation 6) [105]:

$$Ca_d^{MC} = \frac{\eta_d U_{d,MC} l_c}{\gamma_{eq} w_c} \qquad \textit{(Equation 6)}$$

Where Ca_d^{MC} is the microchannel dimension-adapted capillary number of the dispersed phase, η_d is the viscosity of the dispersed phase, $U_{d,MC}$ is the flow velocity of the dispersed phase inside the channel, γ_{eq} is the equilibrium interfacial tension, w_c is the width of the channel, and l_c is the length of the channel.

The wettability of the microchannel walls by the dispersed phase influences the droplet generation; a modified capillary number was proposed to encompass the effect of wettability of the microchannel wall by the dispersed phase (Equation 7) [106]:

$$Ca_d^{\theta} = \frac{\eta_d U_{d,MC}}{\gamma_{eq} |\cos \theta_d|} \qquad \textit{(Equation 7)}$$

Where Ca_d^{θ} is the wettability-adapted capillary number of the dispersed phase, η_d is the viscosity of the dispersed phase, $U_{d,MC}$ is the flow velocity of the dispersed phase inside the channel, γ_{eq} is the equilibrium interfacial tension, and θ_d is the contact angle of the dispersed phase.

The Weber number (Equation 8) is a dimensionless number useful for analysing fluid flow when there is an interface between two fluids [107]. It is a ratio of the fluid's inertial force relative to the interfacial tension force for a given length [107]. The Weber number can be used to determine the maximum stable droplet diameter given the velocity, density, and interfacial tension [107]. As the interfacial tension increases, the maximum droplet diameter will proportionally increase.

$$We = \frac{\rho v^2 l}{\gamma} \qquad \textit{(Equation 8)}$$

Where ρ is the density of the dispersed fluid, v is the dispersed phase velocity, l is the characteristic length (typically droplet diameter), and γ is the interfacial tension.

The area of the channels in relation to the total area of the plate has been reported to be 2 – 6 % for straight-through microchannels [108, 109]. Therefore, fewer channels can be accommodated on a given size of microchannel plate if the channels are larger. With fewer channels, fewer beads are produced from a given size of microchannel plate, so the droplet production frequency is inversely proportional to the size of the microchannels. However, given that larger channels produce larger beads, the production rate of the droplets on a volume basis is independent of the size of the channels [101].

3.0 Objective

The goal of this research was to develop microchannel emulsification for the production of uniform alginate beads with properties suitable for islet cell encapsulation. Specifically, the aims of this project were to:

1) Design and fabricate a microchannel emulsification device
2) Develop an operating procedure for producing alginate beads using the microchannel emulsification device
3) To optimize the process parameters for the production of alginate beads suitable for encapsulation of pancreatic cells

4.0 Materials & Methods

4.1 Microchannel Plates

The microchannel dimensions were chosen based on literature guidelines, and adjusted as needed throughout the process development. A number of plates with varying dimensions were drawn using both AutoCAD (Autodesk, San Rafael, USA) and SketchUp (Trimble Inc., Sunnyvale, USA) software. These microchannel plates were fabricated using various techniques.

4.1.1 Deep Reactive Ion Etching

Deep reactive ion etching was investigated as a method to produce the microchannels through a silicon plate. Deep reactive ion etching allows for the creation of holes or trenches through a substrate with a high aspect ratio. The main advantage of this method over other microelectromechanical methods is that it can produce holes with vertical sidewalls, as opposed to bulbous or tapered walls. To produce the microchannels, the silicon plate would be coated with a masking material, leaving exposed only the areas where a channel was desired. The process then requires alternating between an etching step, in which SF_6 gas is used to etch a thin layer into the

silicon, and depositing a C_4F_8 polymer, which protects the sides of the channels from being etched (Figure 4).

The main limitation of deep reactive ion etching is the rate at which the channel can be etched. In order to etch through a plate that is 500 µm thick or greater, it would take > 8 hours of etching. Consequently, deep reactive ion etching was not considered a viable, cost-efficient method for producing the microchannels.

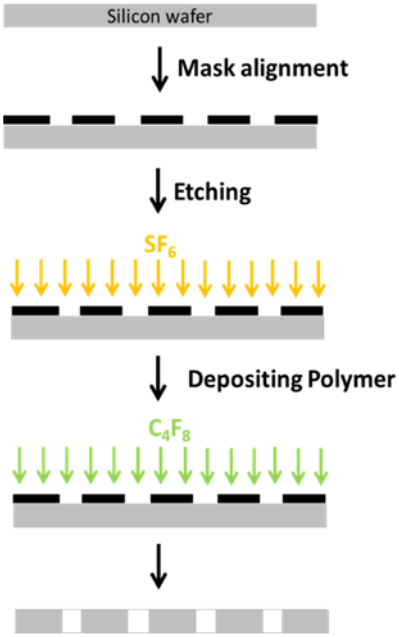

Figure 4. Process to create microchannels using Deep Reactive Ion Etching.

4.1.2 3D Printing

3D printing was investigated as a method to produce the microchannel plates. There are a number of 3D printing facilities that advertise printing capabilities with resolutions as small as 16 µm.

Shapeways 3D printing service (New York City, USA) was used to print the microchannel plates using both Frosted Ultra Detailed Plastic and Frosted Extreme Detail Plastic, both of which are UV-cured acrylic polymers which have the best combination of resolution, ability to print the

size of the piece, and cost. Printing with Frosted Ultra Detailed Plastic is done with 29 µm layers, while Frosted Extreme Detail Plastic is done with 16 µm layers.

The microchannel plate was also printed at the Laboratory for Integrated Prototyping and Hybrid Environments at McGill University using an Objet Connex 500 multi-material 3D printer. The printing process utilizes a technique where a temporary support material, SUP705 acrylic compound, is printed into the space where no final material is meant to be. During the process, the spaces where channels are to be located would be filled with the support material. Once the piece has been printed, the support material must be mechanically removed from the piece.

4.1.3 3D printed mould

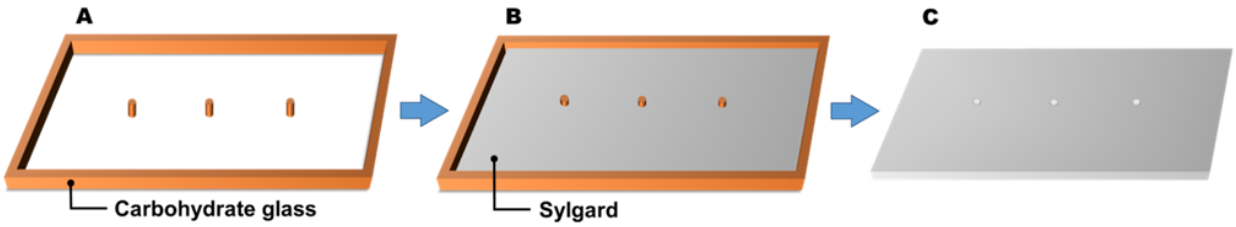

Figure 5. Process to make microchannel plate using 3D printed sacrificial sugar mould. (A) The sugar mould is 3D printed. (B). The silicone is poured into the mould and allowed to set. (C) The sugar is dissolved, leaving the microchannel plate.

Microchannel plates with circular channels were fabricated using a mould. The mould was produced by 3D printing with carbohydrate glass based on a method initially described by Miller *et al.* [110]. This method was adapted by collaborators Prof. Bégin-Drolet and Prof. Ruel at Université Laval to achieve rapid solidification of the carbohydrate glass printing material using a custom 3D printer. A detailed description of the adapted method has been previously described [111]. To produce the microchannel plates, a border for the plate was printed, as well as pillars where the channels were to be. Sylgard (Paisley Products of Canada Inc., Toronto, Canada) was then poured in the mould up to the desired height. Once set, the sugar pillars and border were dissolved, leaving circular microchannels (Figure 5).

4.1.4 Laser micromilling

Laser micromilling was used to produce the microchannels through both polytetrafluoroethylene (PTFE) and fluorinated ethylene propylene (FEP) sheets (McMaster-Carr, Elmhurst, USA) at Potomac Photonics Inc (Halethorpe, USA). Potomac Photonics attempted to mill channels with widths of 100 µm – 200 µm, through sheets with a thickness of 3/32 – 3/16".

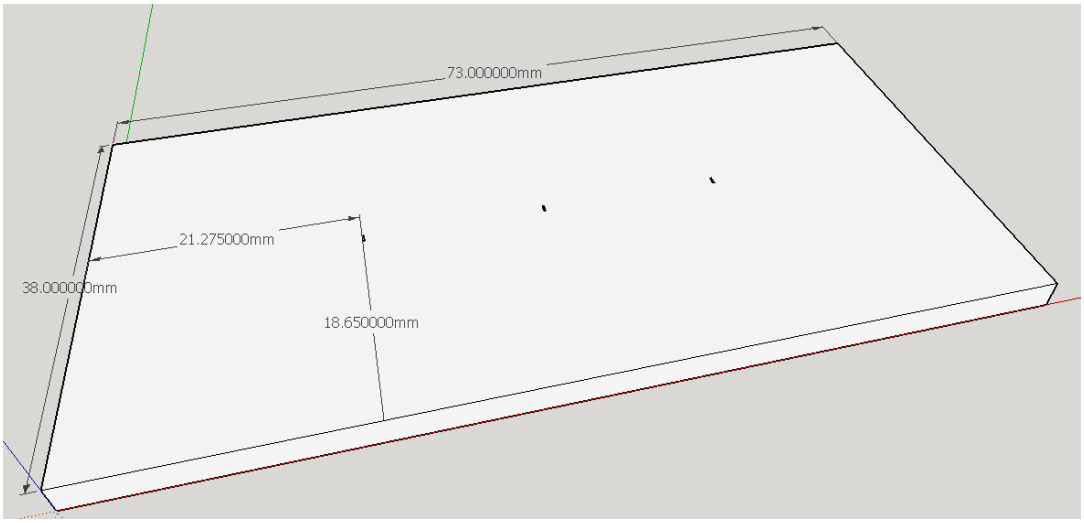

Figure 6. CAD design of microchannel plate to be made from FEP and PTFE.

4.1.5 Determination of water contact angle

An OCA 150 system goniometer (DataPhysics instruments GmbH, Filderstadt, Germany) was used to place a static water droplet on the test material. SCA-20 software was used to capture an image of the profile of the water drop on the solid material and then analyze the angle between the liquid-solid interface and the liquid-vapour interface.

4.2 Flow Chamber System

4.2.1 Light continuous phase design

A microchannel emulsification system was designed to mount the microchannel plate between two flow channels, with the to-be-dispersed phase flowing under constant pressure into the top chamber and the continuous phase under constant flow in the bottom chamber (Figure 7).

This system assumes a continuous phase liquid that is less dense than the alginate. The exit in the top, dispersed phase chamber allows for the system to be purged upon start-up, and is stoppered upon operation to ensure passage of the dispersed phase through the microchannels. The exit of the continuous phase flows to a collection bath, where the alginate beads are collected. The system was designed to allow for time-lapse inverted phase contrast microscopy of the bead formation.

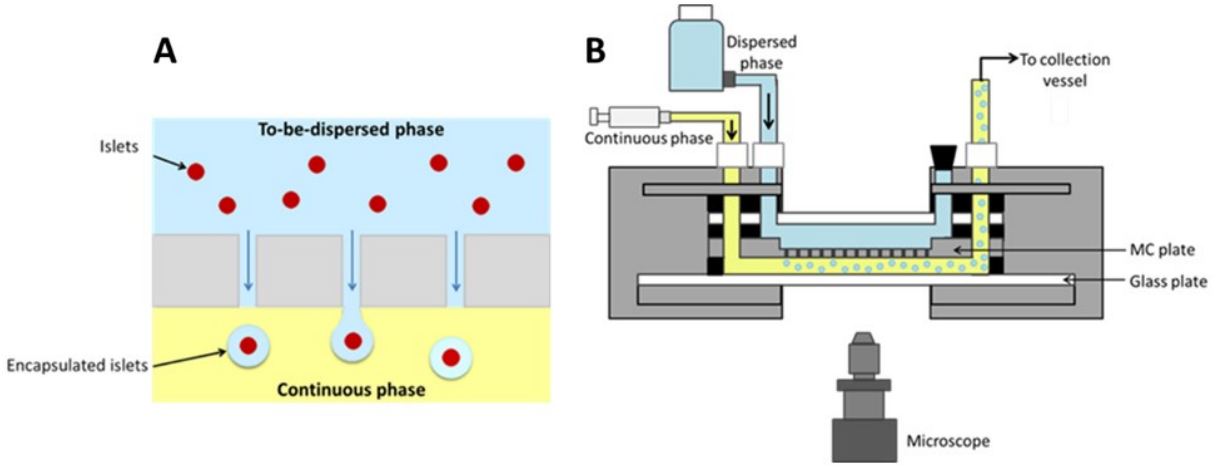

Figure 7. (A) Principle of islet encapsulation by microchannel emulsification described in the light continuous phase design. (B) Microchannel emulsification flow chamber set-up for the light continuous phase design.

The proposed design of the flow chamber system was drawn in SketchUp (Figure 8). The overall dimensions of the apparatus were 120 mm long by 80 mm wide, to enable it to fit in a 96-well plate holder for ease of imaging. The entrances and exits for the flowing fluids were positioned at the top of the system, as opposed to the sides, to ensure the system fit in the plate holder. The height of the apparatus was 7.5 mm so that the bead formation visualization could be kept in focus during imaging.

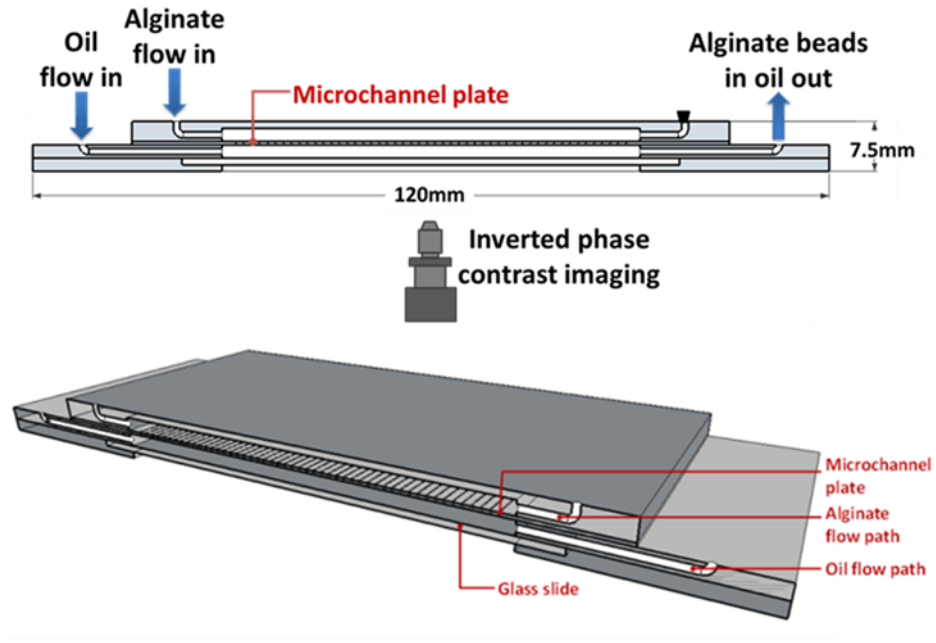

Figure 8. Proposed flow chamber set up design #1.

To test the system shown in Figure 8 prior to fabrication, preliminary flow chamber systems were developed. The first flow chamber system consisted of two small plastic boxes glued to either side of the microchannel plate. To eliminate the need for gluing the system together, an improved microchannel emulsification construction was made using polycarbonate pieces. The bottom and four side pieces necessary to make an open-top box were cut from a piece of 3/8" thick polycarbonate (McMaster Carr, Elmhurst, USA). Openings with 10-32 threading were cut onto the two end pieces of the box. The pieces were then glued together using LePage Stik N' Seal Adhesive (Canadian Tire, Toronto, Canada). Each box had inner dimensions of 2 7/8" x 2 1/8" x 3/8". Two identical boxes were made. A silicone baking sheet (Canadian Tire, Toronto, Canada), approximately 1/16" thick, was cut into 3 5/8" pieces, with an inner, 2 7/8" x 2 1/8" piece cut out, so that the silicone piece covered the top part of the box. The silicone was then glued on the top edge of the polycarbonate box. The boxes had an internal height of approximately 7/16". Once set, the two boxes could be placed on either side of the microchannel plate with the open part

towards the plate. Two clamps were used to hold the boxes and microchannel plate in place, and the pressure on the silicone acted as a seal. Inlet and outlet tubing was connected to both chambers.

4.2.2 Heavy continuous phase design

A second set-up was designed to produce alginate beads using a continuous phase that is denser than the alginate (Figure 9). The alginate flowed in the bottom chamber and the continuous phase in the top chamber, both of which were under constant flow. Given that the alginate beads were less dense and would rise in the continuous phase, the continuous phase exit was located at the top of the chamber, leading to a collection bath above the dual flow chamber.

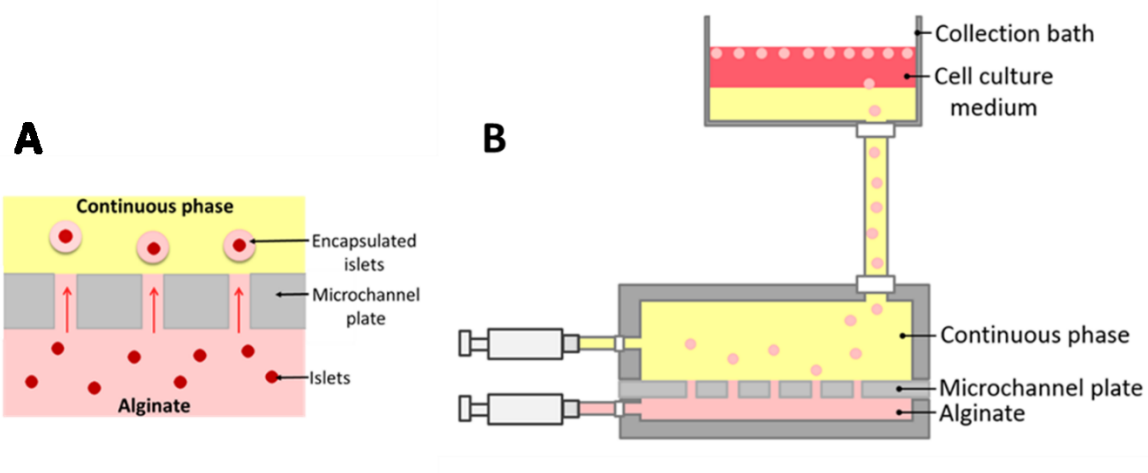

Figure 9. Flow chamber set up for the heavy continuous phase design. (A) Principle of islet encapsulation using proposed design (B) Apparatus set-up

4.3 Selection of Continuous Phase Fluid

4.3.1 Determination of Interfacial Tension and Density

The interfacial tension between alginate and the continuous phase fluid was determined using a DCAT 11 Dynamic Contact Angle Meter and Tensiometer (Particle and Surface Sciences Dataphysics, Gosford, Australia) using the Wilhelmy Plate method at the NanoQAM laboratory (Montréal, Québec, Canada).

The density of the various liquids was calculated using the weight of 25 mL of the liquid. The density difference was then calculated as the absolute value of the difference between the alginate density and the continuous phase density.

4.4 Solution Preparation

All solutions necessary for the production of alginate beads by microchannel emulsification were prepared. The process buffer was prepared, consisting of 10 mM (4-(2-hydroxyethyl)-1-piperazineethanesulfonic acid (Thermo Fisher Scientific, Waltham, USA), 170 mM sodium chloride (Sigma-Aldrich, Saint-Louis, USA), pH 7.4.

The alginate solution was prepared using FMC Manugel® GHB alginic acid (FMC BioPolymer, Philadelphia, USA) dissolved in process buffer in a ratio of 10.5/9 the desired final concentration. For example, for a 1.5% final alginate concentration, 1.75 g of alginic acid was added to 100 mL process buffer. The solution was stirred to dissolve the alginic acid overnight, and autoclaved for 30 minutes.

A 20 mM solution of calcium carbonate (Thermo Fisher Scientific, Waltham, USA) was prepared by adding 1 g of calcium carbonate to 20 mL of process buffer.

All cell culture medium used was Dulbecco's Modified Eagle Medium (Thermo Fisher Scientific, Waltham, USA) with 56.8 mL fetal bovine serum (Thermo Fisher Scientific, Waltham, USA), 5.68 mL penicillin/streptomycin (Thermo Fisher Scientific, Waltham, USA), 5.68 mL 200 mM L-glutamine (Thermo Fisher Scientific, Waltham, USA), and 2 μL of β-mercaptoethanol (Sigma-Aldrich, Saint-Louis, USA) in 500 mL of Dulbecco's Modified Eagle Medium.

The alginate mixture was prepared by mixing 29.7 mL of alginate, 1.65 mL of calcium carbonate solution, and 3.3 mL of cell culture medium, fetal bovine serum, or a combination of the two. If cells were being encapsulated in the alginate beads, the cell culture medium would

contain the desired cell quantity. In some experiments, Tween 20 (Sigma-Aldrich, Saint-Louis, USA) was also added to the alginate.

The acidified continuous phase was prepared by adding acetic acid (Thermo Fisher Scientific, Waltham, USA) to the continuous phase to reach the desired acid concentration. Typically, the acetic acid concentration was 0.22 v/v %.

4.5 Bead Production

To produce alginate beads using microchannel emulsification, the flow chamber system was set up as necessary, either by gluing the two chambers to the microchannel plate, or clamping the system together and connecting the inlet and outlet tubing. The continuous phase was loaded into a BD 60 mL syringe (VWR International, Radnor, USA), the alginate loaded into a 30 mL syringe (VWR International, Radnor, USA), and the syringes attached to the inlet tubing. The syringes were either pushed manually, or with a syringe pump. A Harvard Apparatus PHD 2000 Programmable syringe pump (Harvard Apparatus, Holliston, USA) was used for the continuous phase, and a Sage Instruments model 355 or model 365 syringe pump (Sage Instruments, Freedom, USA) used for the alginate. The bottom chamber was filled with the denser of the two phases, just up to the surface of the microchannel plate. The top chamber was filled with the less dense liquid, the alginate exit tubing was clamped shut, and then both flows started. The continuous phase flow rate was typically between 0 – 70 mL/min, while the alginate flow rate ranged from 2 – 20 mL/min.

4.5.1 Size distribution

To determine the sizes of the beads produced, 0.5 mL of beads were added to 4.5 mL of cell culture medium in a 15 mL centrifuge tube (Sarstedt, Nümbrecht, Germany). Then, 100 µL of saturated Toluidine blue-O (Sigma-Aldrich, Saint-Louis, USA) solution was added to the

centrifuge tube and incubated for one hour on a rotary shaker at 40 rpm. The beads were then filtered on a 40 μm nylon filter (Thermo Fisher Scientific, Waltham, USA) and transferred to a 100 mm diameter Petri dish containing approximately 10 mL of 10% medium in process buffer. Images were acquired using a Samsung Galaxy S4 13-megapixel camera. Bead sizes were obtained via image analysis using the CellProfiler freeware [112].

4.6 Statistics

Statistical analysis was performed with Microsoft Excel software. Multiple comparisons were conducted using one-way analysis of variance. Two-way comparisons were based on Student's t-tests with p-values of 0.05 considered significant.

5.0 Results and Discussion

Several operating parameters affect the microchannel emulsification process. The spontaneous droplet generation process by which droplets of the dispersed phase are pinched off requires specific conditions to sufficiently destabilize the stream of dispersed phase and cause the break-off of uniform droplets. The microchannel dimensions play an important role in the size of the beads that are produced, and the channel length/width aspect ratio is critical to producing uniform droplets. The microchannel plate fabrication material is an important consideration as the continuous phase must preferentially wet the surface of the channels. The continuous phase liquid can be exploited to alter the forces that affect droplet detachment, specifically the buoyancy and interfacial tension forces. Additionally, emulsifiers can be utilized to increase interfacial area, hence promote droplet formation, by decreasing the interfacial tension. All of these parameters were modified in an effort to minimize the alginate bead size and coefficient of variation while simultaneously maximizing the per channel bead production rate. Significant process

modifications and development were required to adapt the stirred emulsification system to produce uniform alginate beads using microchannel emulsification.

Initial attempts to produce alginate beads using microchannel emulsification used the first preliminary system described under the Light continuous phase design (Section 4.2.1). A 500 µm thick Shapeways 3D printed microchannel plate with 500 channels was used. The channels were 240 µm by 640 µm, with a 280 µm space between the long ends of the channels and a 1,000 µm space between the short ends of the microchannels. The continuous phase was mineral oil. Alginate flowed through the channels to form expanding droplets. However, the droplets continued to grow, without detaching from the exit of the microchannel, until they were large enough to touch neighbouring droplets, causing their coalescence into much larger droplets. The larger, coalesced droplets then detached from the microchannel exit (Figure 10). The droplet size was polydisperse, ranging in diameter from under 1 mm to several mm (Figure 11). However, it should be noted that the smaller, < 1 mm droplets did not appear to form during the microchannel emulsification, but rather were shorn from larger droplets as they fell from the exit tubing into the collection bath.

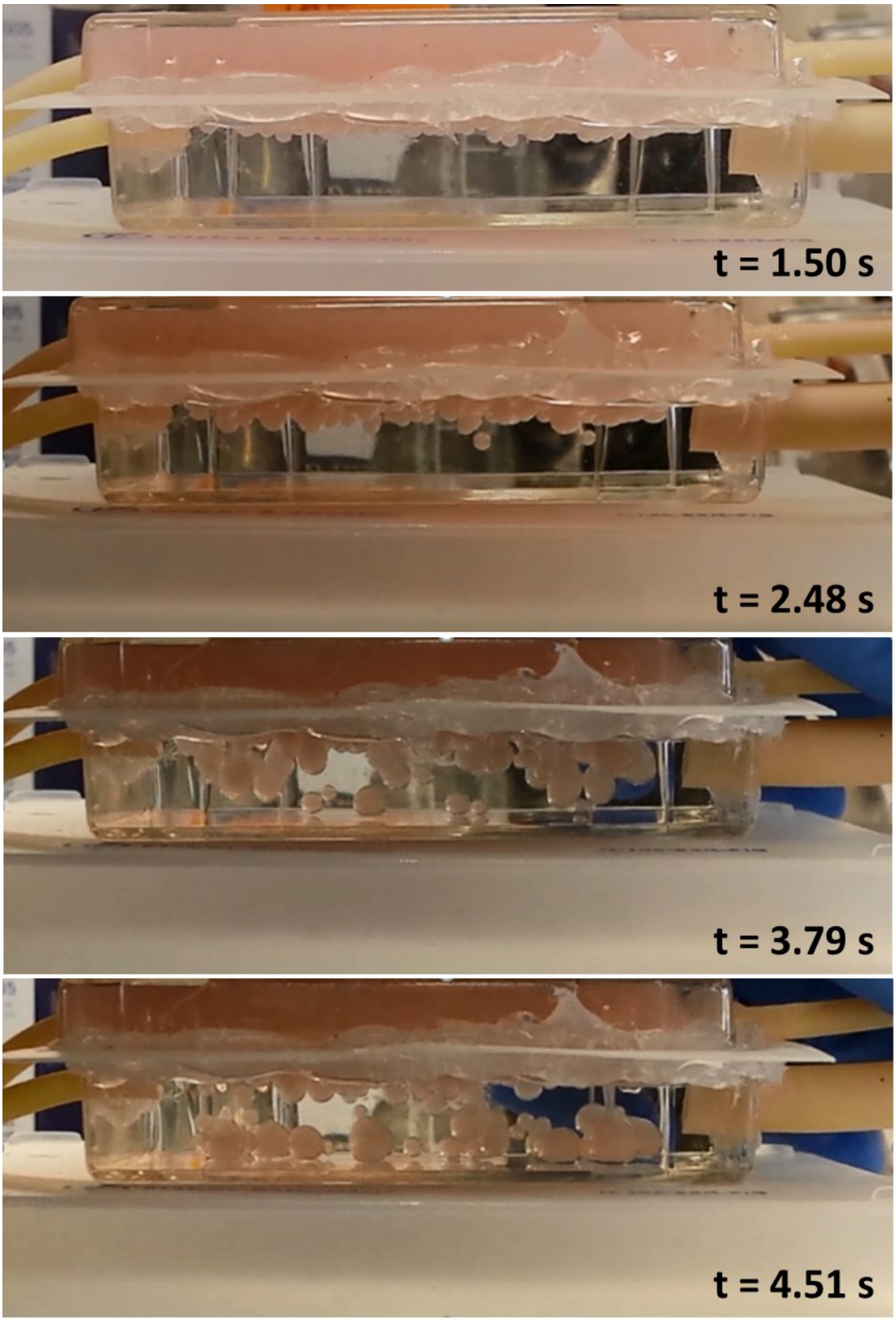

Figure 10. First attempt to produce alginate droplets.

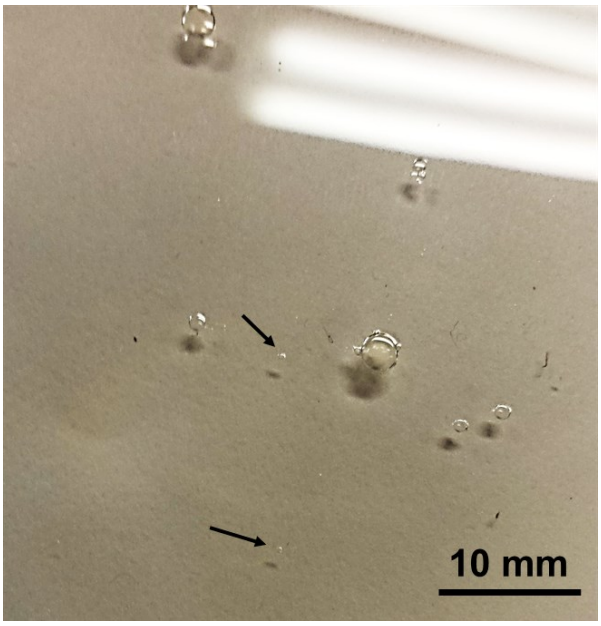

Figure 11. Alginate beads produced during first attempts at microchannel emulsification. Beads with arrows are < 1 mm.

The parameters of this system were not adequate to create the hydrodynamic instability required for proper droplet detachment, which can potentially be attributed to several factors. First, the length/width aspect ratio of the channels was below the specified 3.5 minimum ratio needed to promote detachment of uniform droplets. As well, the hydraulic diameter of the channels was larger than the desired hydraulic diameter. The microchannel plate was made out of a material that was not preferentially wet by the continuous phase. A thin film of the continuous phase on the walls of the channels aids in the formation and pinch off of the dispersed phase neck. Droplet detachment due to hydrodynamic instability would be very difficult to achieve without this thin film. Furthermore, it is likely that the 500 μm length channels did not allow sufficient length for formation of the droplet neck. Without neck formation, any droplet detachment would be due to shear stress from the flow of the continuous phase or steric hindrance from neighbouring forming droplets, both of which result in broad bead sizes. The coalescence of neighbouring droplets suggests there was not adequate space between the channels, but also that the newly formed

interface was sufficiently unstable for droplets to merge. Surfactants could be used to help stabilize the interface. The properties of the continuous phase used in the process could be such that the forces promoting droplet detachment were outweighed by the forces counteracting droplet detachment (Section 2.5). This would be the case if there was a small density difference between the alginate and continuous phase and high interfacial tension. It is likely that all of these factors contributed to the poor droplet detachment observed in the first iteration of the microchannel emulsification process. Further development of microchannel emulsification for production of alginate beads focussed on modifying all of these process parameters.

5.1 Emulsifier type and concentration

Initially, the dispersed phase composition used for microchannel emulsification consisted of an alginate solution supplemented with calcium carbonate and 10% cell culture medium, similar to the stirred emulsification process. When encapsulating cells, the small volume of cell culture medium that is added to the alginate contains the cells. The cell culture medium contains 10% fetal bovine serum, which is added to supply necessary growth factors for cell growth. Moreover, globular proteins and other molecules with amphipathic properties in the fetal bovine serum can act as surfactants and stabilize the emulsion.

In an attempt to facilitate emulsification, the fetal bovine serum-containing cell culture medium that is normally added to the alginate was replaced with 100% fetal bovine serum. The resulting microchannel emulsification attempt is shown in Figure 12. The alginate flowed through the channels, but rather than breaking off into droplets, a continuous outflow and expansion of the alginate was observed. Various fetal bovine serum to cell culture medium ratios were tested. Use of either cell culture medium alone or fetal bovine serum alone resulted in the continuous outflow of the alginate from the channels with no detachment of the flow. However, a combination of both

fetal bovine serum and cell culture medium resulted in periodic break off of the flow, resulting in large alginate drops of ~1 cm in diameter. A combination of 1 mL of fetal bovine serum and 2.3 mL of cell culture medium was found to increase the tendency of the alginate flow to break off. For this 1:2.3 ratio, the final volumetric concentration of fetal bovine serum in the dispersed phase preparation is 3.5% compared to 1% for medium alone or 9.5% for fetal bovine serum alone. Adding surfactant had a stabilizing effect on the emulsion, however it is possible for the alginate-oil interface to be stabilized too much. Over-stabilization of the interface will decrease the thermodynamic need for the alginate to transform into spheres. This over-stabilization, when 100% fetal bovine serum is added, is observed as jetting of the alginate. Moderate addition of surfactant allows for adequate stabilization, resulting in droplet production. However, other microchannel emulsification parameters needed to be modified to promote droplet detachment into smaller beads.

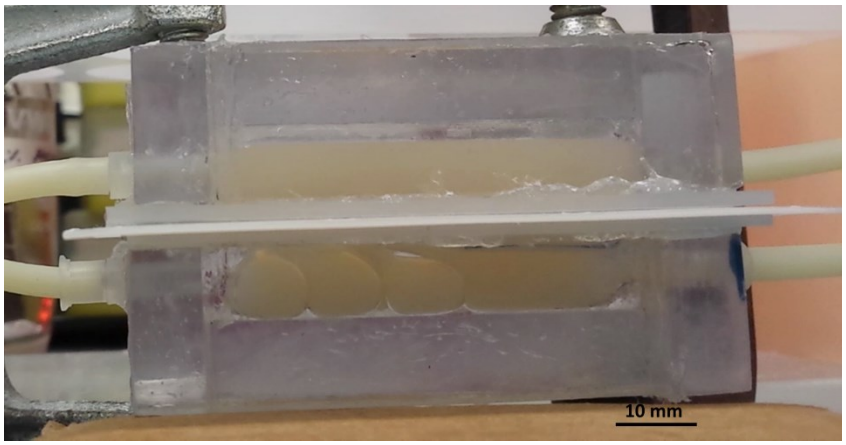

Figure 12. Microchannel emulsification with improved flow chamber system.

Tween 20 is a polysorbate-type, non-ionic surfactant suitable for use in cell culture that was tested as an alternative surfactant based on its known surface-stabilizing properties. Tween 20 was added to the to-be-dispersed alginate phase in concentrations ranging from 0.05 v/v % to 0.5 v/v %. Concentrations of 0.05% did not appear to affect the bead size. However, a

concentration of 0.5% resulted in beads with a broad size distribution. While most of the beads were between 3 – 7 mm in diameter, some beads of approximately 0.5 mm diameter were obtained.

Overall, the addition of 1 mL of fetal bovine serum and 2.3 mL of culture medium (which contains 10% serum) per 34.65 mL total dispersed phase preparation volume was the most promising surfactant for bead formation as it appeared to adequately stabilize the interface. This ratio of fetal bovine serum to cell culture medium was used for all subsequent experiments, unless otherwise noted.

5.2 Continuous phase selection

The properties of the continuous phase used for the emulsification can significantly facilitate droplet break-off. Equation 3 shows that the buoyancy force promoting droplet detachment is proportional to the density difference between the continuous and dispersed phase. Therefore, the ideal continuous phase would have a large density difference with alginate. The interfacial tension force (Equation 4) is proportional to the interfacial tension between the continuous and dispersed phase, and works to counteract droplet detachment. A continuous phase liquid that has a minimal interfacial tension with alginate is necessary to produce smaller alginate beads. The microchannel emulsification process was developed with the goal of encapsulating cells for transplantation. It is important, then, that the continuous phase liquid is cell-friendly, and ideally also previously approved for transplantation applications by regulatory agencies.

The current work was based on modifying the stirred emulsification process to directly produce the dispersed phase droplets. As such, initial work to develop microchannel emulsification used light mineral oil as the continuous phase, similar to the stirred emulsification process. Sunflower oil, grapeseed oil, and walnut oil were then tested as alternative continuous

phases. Novec 7500 Engineered Fluid, a product by 3M, was also investigated as a continuous phase.

The interfacial tension between alginate and all alternative continuous phases was lower than the interfacial tension between alginate and mineral oil (Figure 13). Sunflower oil, grapeseed oil, and walnut oil all had respectively lower interfacial tensions with alginate. The Novec 7500 fluid also had a decreased interfacial tension, second only to the walnut oil. The density difference of the three oils was slightly lower than that of the mineral oil, whereas the density difference of Novec 7500 fluid was approximately four-fold higher than that of the mineral oil (Figure 14). Perfluoro(methydecalin) also has a high density difference, almost 6.5 times higher than mineral oil. All three oils are non-toxic, with prominent applications in the food industry. Novec 7500 Engineering Fluid exhibits a very low overall toxicity, exhibiting no adverse effects at 1000 mg/kg body weight in a 28-day oral toxicity study [113]. However, none of these three fluids are currently approved for transplantation applications. Perfluoro(methyldecalin) is chemically and biologically inert, and already used in transplantation applications [114]. Although not tested experimentally, perfluoro(methyldecalin) may represent a promising alternative for transplantation applications.

There was no change in alginate bead size when using sunflower oil, grapeseed oil, or walnut oil compared to mineral oil. Use of the Novec 7500 fluid as the continuous phase resulted in a significant decrease in the alginate bead size. As the Novec 7500 fluid is denser than the alginate, the set-up had to be inverted, with the continuous phase in the bottom chamber and the alginate in the top chamber, as described in the heavy continuous phase design. The laser micromilled PTFE plate was used, as it had the highest water contact angle and channel length/width aspect ratio. The Novec 7500 continuous phase significantly improved droplet

formation, and resulted in beads that were approximately 3 mm in diameter with a coefficient of variation of 9.3 %, the smallest beads yet (Figure 15).

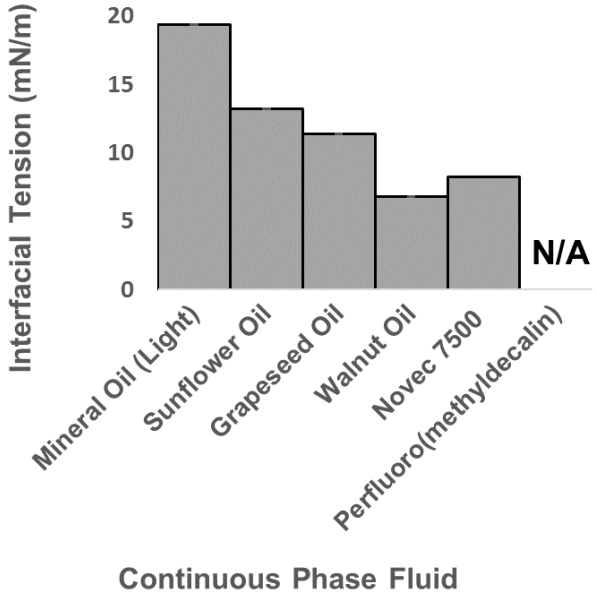

Figure 13. Interfacial tension between continuous phase fluids and 1.5% alginate mixture.

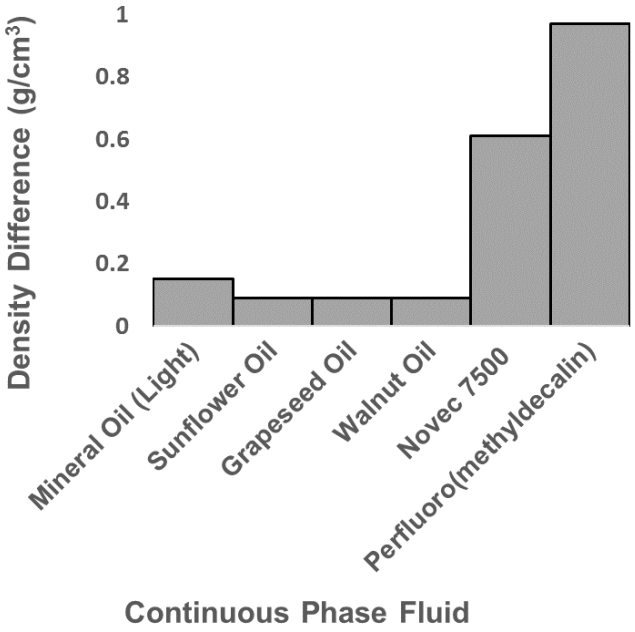

Figure 14. Density difference between continuous phase fluids and 1.5% alginate.

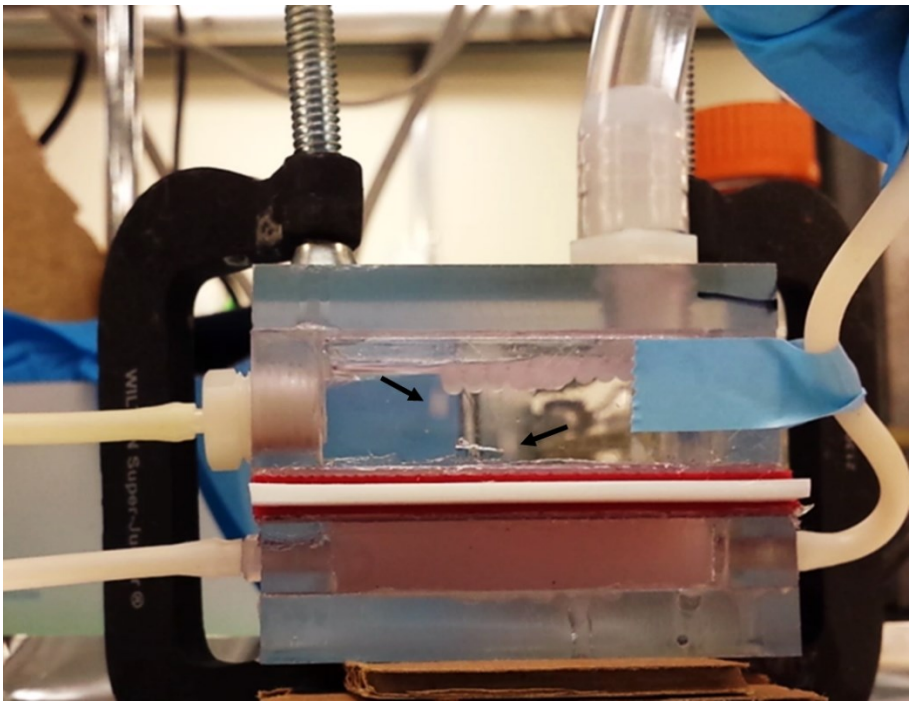

Figure 15. Bead production using laser micromilled PTFE microchannel plate and Novec 7500 fluid. The arrows highlight a rising droplet that will exit through the top chamber exit. Other beads that did not exit the chamber are visible in the chamber.

Modification of the continuous phase liquid was the final modification needed to successfully produce alginate beads using microchannel emulsification. The alginate beads shown in Figure 16 were produced using the Novec 7500 Engineering fluid and the laser micromilled PTFE microchannel plate. The average bead diameter was 2.9 mm, with a coefficient of variation of 9.3 %. These conditions also resulted in the highest droplet production frequency. Approximately 5 beads/s/channel were produced, corresponding to a production rate of 4 mL/min/channel.

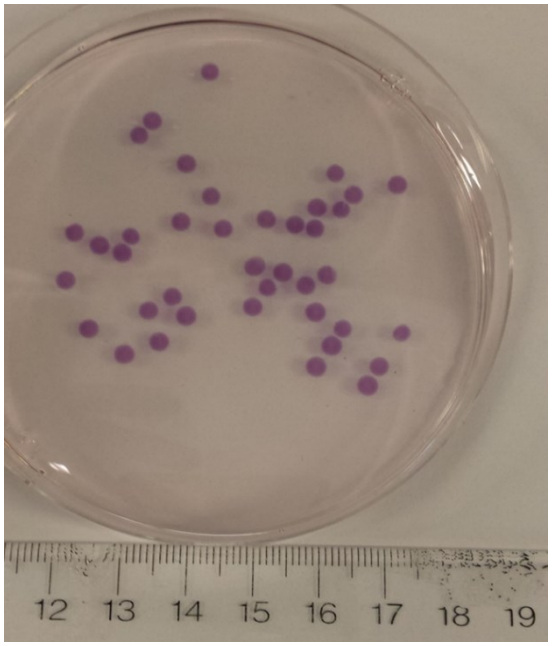

Figure 16. Toluidine Blue-O stained alginate beads produced by microchannel emulsification with Novec 7500 fluid.

Equation 3 and Equation 4 show that increasing the bead diameter should have greater impact on the buoyancy force compared to the interfacial tension. The sunflower oil, grapeseed oil, and walnut oil all had lower interfacial tensions than mineral oil. However, the benefit of the decreased interfacial tension was outweighed by the decreased density difference, explaining why no improvement to the alginate bead size was observed. Novec 7500 fluid did not have the lowest interfacial tension of the continuous phases tested, but the considerably increased density difference with alginate aided greatly in promoting droplet detachment at smaller bead sizes. Previous work to produce water-in-oil emulsions using microchannel emulsification used decane [115] or iso-octane [116] as the continuous phase, which have a density difference with alginate of ~0.27 g/cm^3 and ~0.31 g/cm^3, respectively, both of which are higher than any alginate and oil combination. This suggests that a higher density difference is a crucial parameter in promoting droplet detachment. However, both decane and iso-octane are highly flammable and toxic when ingested, and are thus not suitable for cell encapsulation and transplantation applications. Novec

7500 fluid has improved properties as a continuous phase compared to both decane and iso-octane, as it has a higher density difference and is non-toxic. Future work could investigate perfluoro(methyldecalin) as a possible continuous phase liquid. Perfluoro(methyldecalin) is a perfluorocarbon liquid, which are hydrocarbons in which most or all of the hydrogen atoms have been replaced by fluorine atoms. Perfluorocarbons are currently used in a variety of transplantation applications, including pancreas preservation for pancreas and islet transplantation applications [117]. *In vitro* culture of rat islets in culture medium with 3.5 w/v% perfluorocarbons maintained islet viability and improved islet functionality [118]. The safety of perfluorocarbons, combined with their high density difference with alginate, make them a promising continuous phase for promoting droplet detachment in microchannel emulsification.

5.3 Microchannel plate material and dimensions

5.3.1 Microchannel plate properties

In addition to the forces promoting droplet detachment, the material and dimensions of the microchannels play an important role in detachment of uniform droplets of a specific size. Literature suggests that microchannels with a channel length/width aspect ratio of 3.5 will result in uniform droplets with a diameter of twice the hydraulic diameter [97]. Typical microchannel plates are between 200 – 500 μm thick. Along the length of the channel, the dispersed phase is destabilized, leading to the formation and pinch-off of the dispersed phase neck. It was hypothesized that increasing the length of the channels by increasing the thickness of the plate would aid in droplet detachment, as it would allow for a greater length to destabilize the alginate flow and allow for formation and pinch off of the neck. The pinch-off of the neck also requires that the continuous phase preferentially wet the surface of the microchannels. To produce alginate

beads in a non-aqueous phase, the microchannel plate should be made out of a hydrophobic material, represented by a water contact angle exceeding 90°.

The first microchannel plate design had 200 μm by 700 μm straight-through channels across a 500 μm thick plate. These dimensions correspond to a channel aspect ratio of 3.5 and a hydraulic diameter of 311 μm. The expected minimum bead diameter that can be obtained in optimal operating conditions from such channels is 600 μm in diameter. Shapeways was able to successfully print a plate with oblong channels using the Frosted Ultra Detail Plastic (Figure 17), one of the company's proprietary materials. However, the channels were not rectangular, 200 μm by 700 μm channels, but oval-shaped channels with dimensions of 240 μm by 640 μm, on average. Printing the microchannel plate with the highest resolution material, Frosted Extreme Detail Plastic, resulted in the material caving in and completely blocking the channels. In an attempt to reduce the channel width of the Frosted Ultra Detail Plastic plates, designs with 150 μm and 100 μm width channels were submitted. The designs with 150 μm channels did not result in narrower channels, while the designs with 100 μm width channels resulted in the channels being completely obstructed by the plastic after the printing process. In order to enhance pinch-off of the dispersed phase in the channel, attempts were made to 3D print thicker microchannel plates. Shapeways successfully printed 1 mm thick plates; however, 2 mm, 3 mm, and 5 mm plates resulted in blocked channels. The number of channels per plate was also decreased, with a minimum of 3 mm between each channel, to facilitate the visualization of the droplet formation. The water contact angle of the 3D printed Frosted Ultra Detail Plastic plates was 70°, lower than the desired minimum contact angle of 90°. While there was moderate success producing the microchannel plates with this method, the main drawbacks were the limited control over the width of the microchannels and the thickness of the plates, as well as the low water contact angle of the material.

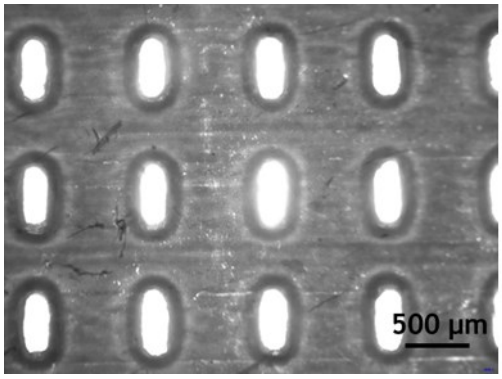

Figure 17. Polymer microchannel plate 3D printed by Shapeways.

Alternative 3D printing facilities were tested to determine if the microchannel plates could be produced with greater control over the dimensions of the microchannels. The Laboratory for Integrated Prototyping and Hybrid Environments used a printing process that consisted in printing a temporary support material in the locations of the eventual channels at the same time as printing the surrounding plate material. Once the printing is complete, the support material is removed to create channels. However, as the channels were very small, it was not possible to remove the support material from the space where the channel was meant to be. The channels were completely filled in with the support material, rendering them unusable.

An alternative to 3D printing the microchannel plate directly would be to print a mould using a sacrificial material and cast the plate material around the mould. A microchannel plate was produced by 3D printing a carbohydrate glass (sugar) mould including pillars, casting silicone into the mould, curing the silicone, then dissolving the carbohydrate glass. Sugar is biocompatible and easy to dissolve, making it an ideal material for a sacrificial mould. This microchannel plate was produced in collaboration with the group of Dr. Begin-Drolet. Producing the microchannels using a carbohydrate glass mould successfully produced circular microchannels (Figure 18). The diameter of the channels is determined by the diameter of the 3D printed carbohydrate glass pillars. A 0.5 mm diameter nozzle was used to print the carbohydrate glass pillars, and the printed pillars

had a diameter larger than the diameter of the nozzle. The microchannels in Figure 18 were, on average, 750 µm in diameter through a 4 mm thick plate. The advantage of this method is that the height of the plate can be increased without compromising the microchannels. This method was also used to make the microchannel plate out of silicone, which has a water contact angle of 95°, significantly higher than the water contact angle of the 3D printed microchannel plates. However, because the mould for the channel was printed with a circular nozzle, the microchannels produced using this method were circular, rather than oblong, which was the main drawback to this method. If it were possible to retrofit the printer with an oblong nozzle to produce oblong microchannels, this would be a very promising method to produce the microchannel plates.

Figure 18. Silicone microchannel plate with circular microchannels produced using 3D printed sugar mould.

Laser micromilling was considered as an option to obtain rectangular channels through mm-thick materials. Potomac Photonics succeeded in milling channels through 2.4 mm thick sheets of both PTFE (Figure 19) and FEP. The design specified channels of 200 µm by 700 µm. However, the edges of the channels were rough and the size of the channels was not precise. The channels were, on average, 488 µm by 928 µm. PTFE has a water contact angle of 109.2° [119], while FEP has a water contact angle of 108.5° [119]. The laser used to mill the channels was unable to mill thinner, 150 µm width channels. Additionally, it was not possible to mill through 3.2 mm or 4.8 mm thick sheets of PTFE and FEP. The main benefit of the laser micromilling method is that it allowed for the production of microchannel plates that were made from a hydrophobic material and had microchannels with dimensions allowing alginate droplet break-off.

However, there was still poor control over the size of the microchannels, as the hydraulic diameter was over two times the intended hydraulic diameter. The rough edges of the laser micromilled channels may also impact the droplet detachment behaviour. The rough channel walls could increase the turbulence of the alginate within the channel, thereby artificially increasing the capillary number and promoting alginate jetting.

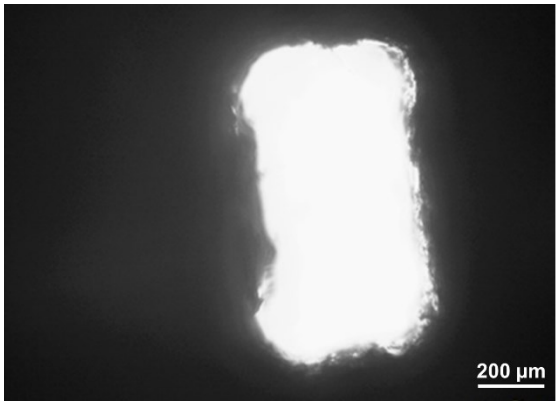

Figure 19. Microchannel laser micromilled through 2.4 mm thick PTFE sheet.

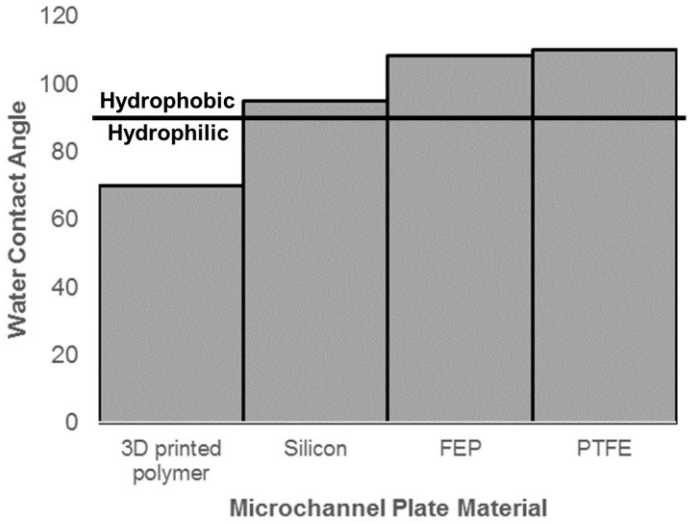

Figure 20. Water contact angles on different microchannel plate material.

Table 2. Properties of tested microchannel plates

Plate Material	Water Contact Angle (°)	Channel Hydraulic Diameter (µm)	Channel Aspect Ratio (length/width)	Channel Length (mm)
Acrylic polymer	70	349	2.7	1
Silicone	95	750	1	4
PTFE	110	640	1.9	2.38

Table 2 summarizes the properties of the microchannel plates made using the three techniques described above. The acrylic polymer and silicone plate were created directly with the channels, whereas the PTFE plate was made by creating channels through a solid piece. The acrylic polymer 3D printed plate was relatively inexpensive and easy to make, though posed limitations to the minimum channel width and maximum channel length possible. Furthermore, precise control of the channel dimensions was not possible, and the plate was made out of a hydrophilic material. The silicone plate made using a sacrificial carbohydrate glass mould overcame the limitation to the channel length and was hydrophobic. However, only round channels could be made, with a hydraulic diameter considerably larger than desired. Finally, the PTFE laser micromilled plate allowed the production of rectangular channels through thicker plates than the acrylic polymer plate. PTFE had the highest water contact angle. However, there was still limited control over the size of the microchannels, resulting in a lower channel length/width aspect ratio and higher hydraulic diameter than desired. Still, the PTFE plate represented the best combination of parameters. Future work should focus on laser micromilling through PTFE with high precision and size control.

5.3.2 Influence of microchannel plate on bead production

Use of the first 3D printed microchannel plate resulted in the continuous outflow and expansion of the alginate. To minimize this, alternate microchannel plates were used. As

previously stated, a longer channel length would increase the hydrodynamic instability, thus promote droplet detachment. The thickness of the microchannels plate was therefore increased from 500 μm to 1 mm, which significantly improved droplet detachment. Indeed, rather than the continuous outflow and expansion of the alginate, droplets detached from the surface of the plate into the continuous mineral oil phase. Highly uniform beads of approximately 4 – 5 mm in diameter were formed. Figure 21 shows the production of these droplets.

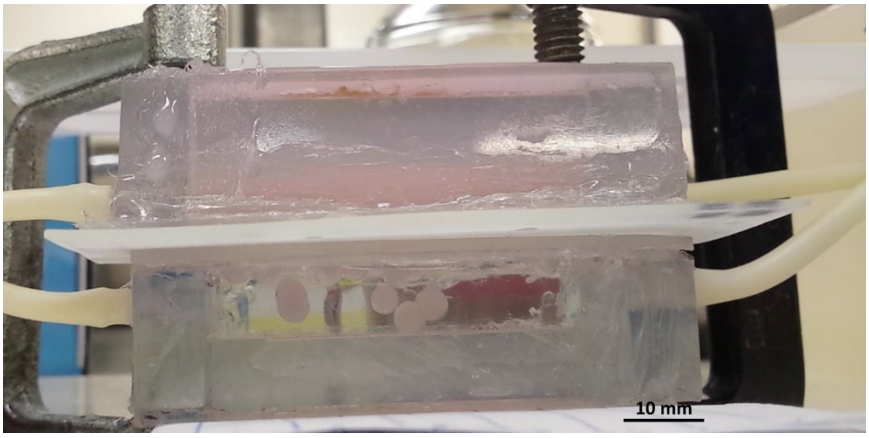

Figure 21. Microchannel emulsification after process improvements.

Three flow regimes were observed with increasing dispersed phase flow: uniform bead formation, irregular bead formation, and jetting. The uniform bead formation regime exists below a critical capillary number, where interfacial tension is the dominant force driving droplet formation. Viscous force effects become significant above the critical capillary number. The critical capillary number will vary for each system, and must be determined with each change in operating parameter. Various flow rates were tested to determine the regime resulting from the operating conditions (Figure 23). Given the alginate flow rates that produced uniform beads compared to irregular beads, the critical capillary number for this system was between 1474 – 1842. At a capillary number of 1474, the system operated in the uniform bead formation

regime, whereas irregular bead formation occurred at 1842 capillary number. Further experiments between these capillary numbers would be needed to determine the exact critical capillary number.

Since increasing the channel length from 500 μm to 1 mm significantly impacted droplet detachment, attempts were made to further increase the channel length. It was not possible to increase the channel length using the 3D printed plates, so the sugar moulded plates were used. Alginate beads were successfully produced using the 4 mm-thick moulded plate (Figure 22). The beads were approximately 4.9 mm in diameter and were highly uniform, with a coefficient of variation of 5.4%. There did not appear to be a significant difference in bead size between the beads produced using the 3D printed plate or the silicone plate based on visual observation.

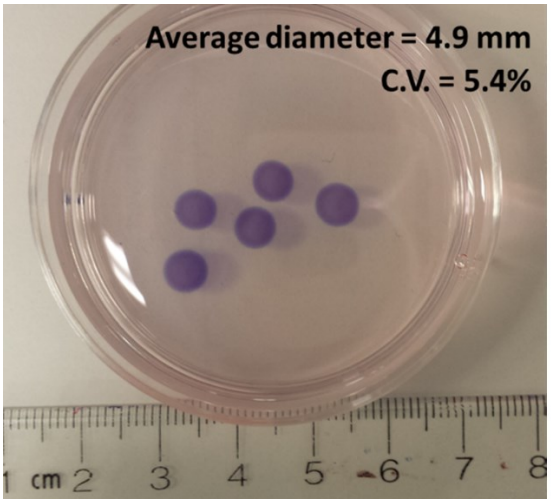

Figure 22. Alginate droplets produced using 1 mm thick microchannel plate, stained with Toluidine Blue-O.

The flow behaviour was tested to compare the bead formation using both the 1 mm thick 3D printed plate and the 4 mm thick silicone plate. Uniform bead formation was observed at higher channel flow rates, hence higher capillary numbers, with the silicone plate than the 3D printed plate (Figure 23).

The silicone plate had an increased channel length and water contact angle, but the 3D printed plate had a higher aspect ratio. In an effort to combine the benefits of both of these plates,

the laser micromilled plates were produced. Both the PTFE and FEP laser micromilled plates successfully produced uniform alginate beads of ~4 mm in diameter.

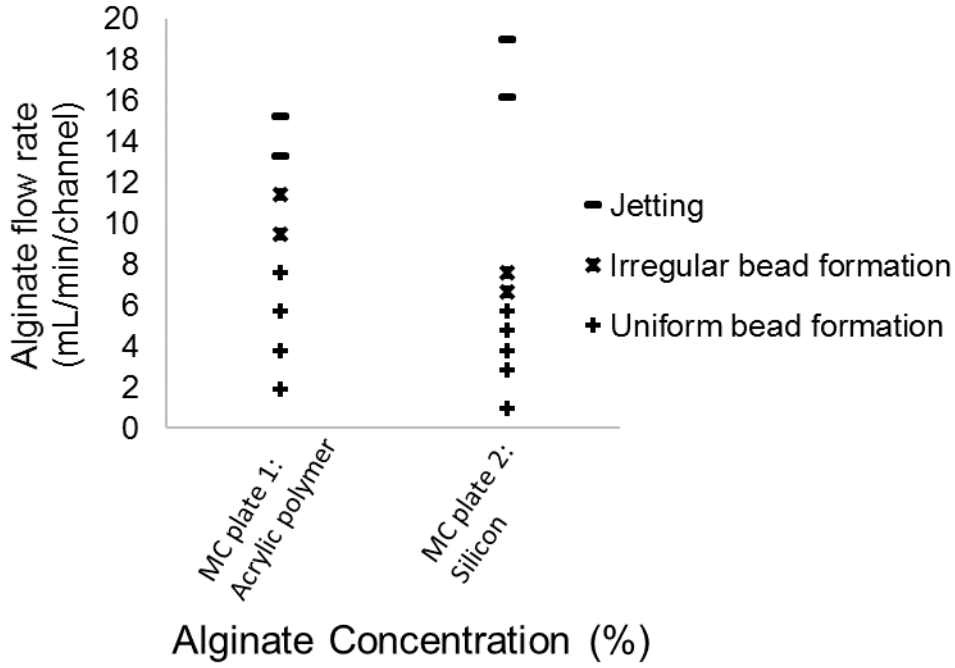

Figure 23. State diagram of bead production by microchannel emulsification.

5.4 Emulsification apparatus design

The first emulsification apparatus used a clear plastic box glued to either side of the microchannel plate, as seen in Figure 10. This approach required that the apparatus be cut open for cleaning and then reassembled with glue after each experiment. This process was tedious and time consuming. The polycarbonate box system, described in section 4.2, was then made to eliminate the need to glue the apparatus together. However, the continuous phase chamber was not tall enough to accommodate the forming beads. Once alginate droplets accumulated at the bottom of the chamber, the new droplets did not have adequate space to detach. As well, the alginate droplets were too large to flow through the outlet tubing. To address these issues, new polycarbonate boxes with an increased continuous phase chamber height and increased outlet

diameters for the continuous phase chamber were made. The continuous phase flow chamber was increased from 11.1 mm in height to 20.6 mm. The outlet tubing had a minimum internal diameter of 8 mm, wide enough to accommodate the 3 – 5 mm alginate beads.

After modifying the continuous phase liquid to use Novec 7500 fluid (Section 5.2), the apparatus was further modified to allow the alginate beads to float up and away from the microchannel plate. As the Novec 7500 fluid is denser than the alginate, the set-up was inverted to have the continuous phase in the bottom chamber and the alginate in the top chamber, as described in the heavy continuous phase design (Section 4.2.2). In the current apparatus, the beads detach and float up into a collection bath located above the chambers. Alginate beads were successfully produced and collected using this system. However, certain design aspects of this prototype should be improved. For example, the system requires clamps to seal and hold the chambers together. The imperfect seal sometimes results in leaks between the continuous phase chamber and the microchannel plate. As well, changes to the applied pressure would slightly change the height of the chambers between experiments. Future work should include machining of a flow chamber system that uses o-rings for seals and is screwed together. Proper sealants and distribution of the pressure holding the chambers together should prevent any leaks and ensure a constant chamber height.

5.5 Alginate flow rate and concentration

Having achieved uniform bead production, the alginate flow rate and concentration could be tested to determine the process operating range of these parameters. The size of the alginate beads should be constant up to a critical capillary number. Therefore, the bead sizes should be

uniform and independent of the alginate flow rate and concentration up to a certain point, above which continuous outflow and expansion is observed.

The effect of the alginate flow rate on the bead size was determined for a flow rate range of 2.6 mL/min – 4.5 mL/min at a low, mid, and high flow rate (Figure 24). The beads produced at each of the operating conditions were very uniform in size, with coefficients of variation between 1 – 6 %. Contrary to expectations, preliminary data suggested that the flow rate impacted the bead diameter; operating at a mid flow rate produced beads that were significantly larger than the beads produced at the low and high flow rate. However, the error bars shown in Figure 24 represent the standard deviation of the size of the beads from one experiment, rather than standard error of the means of experimental replicates. The flow rate effect is therefore currently confounded with the variability between experiments. If further experimental replication shows a significant trend, this change in bead size with dispersed phase flow rate could be explained by various forces becoming dominant at different flow rates. For example, increasing the dispersed phase flow rate would increase the inertial force promoting droplet detachment, but also increase the drag force counteracting droplet detachment. The current variability in bead size as a function of flow rate represents only a 14% change in diameter between the largest and smallest sizes. Even if the effect of alginate flow rate on bead size is found to be significant after experimental replicates, the magnitude of this effect is relatively small over the flow rate range tested.

The alginate bead sizes were determined with varying alginate concentrations, from 0.5 % alginate to 2.5 % alginate, at a low, mid, and high point (Figure 25). The beads produced at each of the three conditions were again very uniform in size, with coefficients of variation between 1 – 3 %. However, a significant difference in bead size between all three conditions was observed, with beads ranging from 2.6 mm to 3.5 mm in diameter. Again, the error bars represent the

standard deviation of the size of the beads from one experiment, so further replicates are needed to determine if the trend is significant. A significant trend of bead size increase then decrease with increasing alginate concentration could be explained by the balance of viscous and interfacial tension forces that become dominant with increasing alginate concentration.

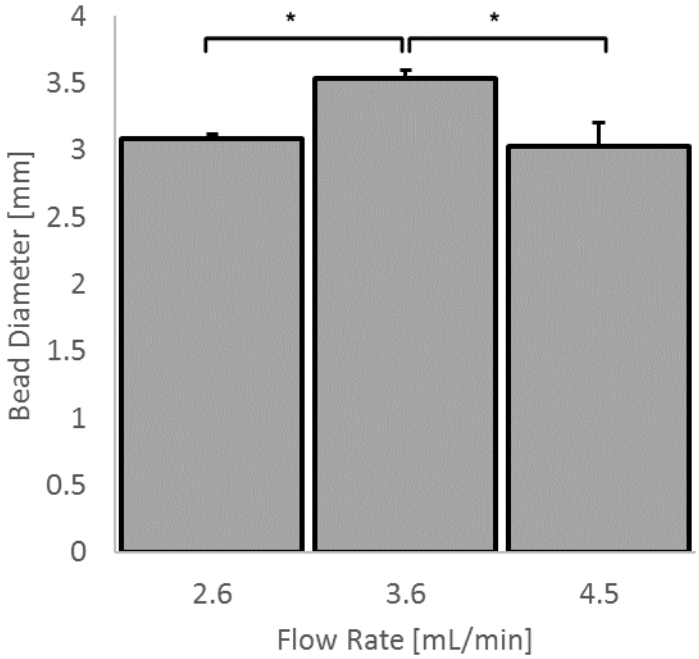

*Figure 24. Effect of alginate flow rate on bead diameter. Error bars are standard deviation of n=10 beads. *p<0.05*

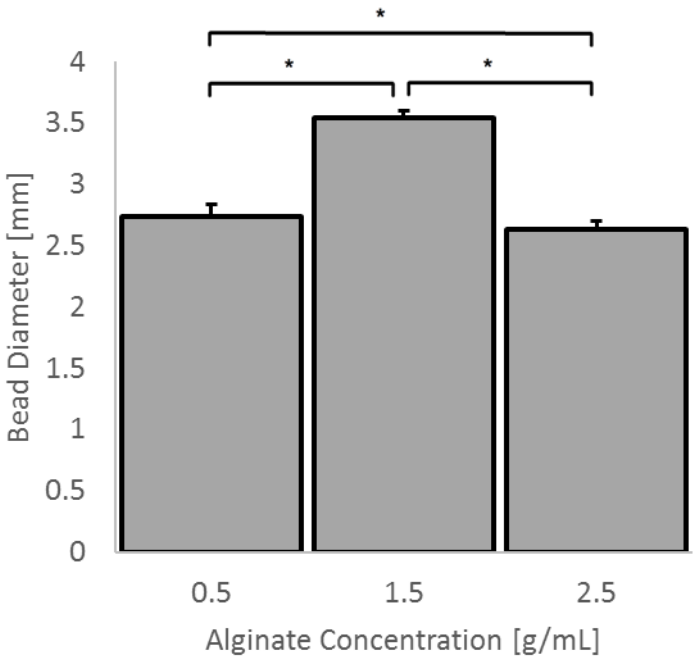

*Figure 25. Effect of alginate concentration bead diameter. Error bars are standard deviation of n=10 beads. *p<0.05*

Though the bead sizes appear to vary with variation in alginate flow rate and concentration, this is likely the result of experimental and operator variation. To run an experiment, the bottom chamber is first filled with alginate until it reaches the surface of the microchannel plate, prior to filling the top chamber with the continuous phase. It is difficult to control precisely how far through the channel the alginate is first filled. The time that the alginate spends in contact with the channel surface also varies between experiments. These two parameters would influence the wettability of the continuous phase on the channel surface, influencing the dynamics of neck formation and pinch-off. Visual observation showed that these factors influenced the size of alginate beads that are produced. This could account for the variation in bead size that was observed with changing alginate flow rate and concentration. Improving the apparatus design may reduce both the experimental and operator variability. An improved design could allow for the continuous phase to be filled into the chamber first, followed by the alginate, which would

minimize variability in the wettability of the continuous phase on the microchannel surface. Moreover, the temperature of the alginate was not accounted for in these experiments. Both the 0.5 % and 2.5 % alginate were used at approximately room temperature, while the 1.5 % alginate was used while cool, at approximately 4 ^{o}C. The temperature of the alginate affects the viscosity of the alginate, so it is likely that the 1.5 % alginate was disproportionately viscous compared to its concentration. This could have played a role in producing beads that were larger than expected. Temperature effects and between-operator effects on the bead size should be assessed. After accounting for temperature and wettability effects, it is expected that experimental replicates would show no significant trend of alginate flow rate and concentration on bead size.

5.6 Current operating parameters and bead production rates

Significant process development of the microchannel emulsification system has resulted in a process that can produce uniform alginate beads. A combination of modifications to the microchannel plate dimensions and material, continuous phase liquid, surfactant, and apparatus design was necessary. The current process uses a laser micromilled PTFE microchannel plate, and Novec 7500 fluid as the continuous phase. The parameters of bead production using the current microchannel emulsification system are summarized in Table 3.

Table 3. Parameters of bead production using current microchannel emulsification system.

Bead diameter (mm)	**Coefficient of Variation (%)**	**Dimensionless Droplet Diameter**	**Bead Production Frequency (s^{-1})**	**Bead Production Rate per channel (mL/min/channel)**	**Overall Production Rate ($L/m^2/h$)**
2.9 ± 0.3	9.3	4.6 ± 0.4	5	4	17,495

The current channel dimensions and spacing allow for 72,898 channels on a 1 m^2 microchannel plate. Given current per channel production rates, this corresponds to an overall production rate of 17,495 L m^{-2} h^{-1}. This production rate is an improvement to previously reported

microchannel emulsification production rates of up to 1, 200 L m^{-2} h^{-1}, and exceeds production rates of current cell encapsulation methods (Table 1). Given that approximately 100 mL of alginate beads is required to treat one patient, enough beads could be produced for a patient in just one minute with only 25 channels.

A coefficient of variation of 9.3% is significantly improved from the stirred emulsification method, which can have a coefficient of variation over 40 %. However, this value is higher than reported values for microchannel emulsification systems, where coefficients of variation are less than 5 %, and can be as low as >2%. The coefficient of variation obtained was also higher than reported coefficients of variation for microfluidic devices, but lower than typical membrane emulsification systems. The current coefficient of variation of 9.3 % is similar to values reported for nozzle-based devices [120].

The current microchannel aspect ratio of 1.9 falls short of the reported aspect ratio of 3.5 necessary to produce uniform droplets. Thus, the high coefficient of variation can be attributed at least in part to the current channel dimensions. Furthermore, the bead size depends on the microchannel size. It is likely that the lack of precision of the microchannel dimensions contributed to the droplet size variability.

The current dimensionless droplet diameter, the droplet diameter normalized to the channel hydraulic diameter, is 4.6 ± 0.4, higher than values of 2 reported in literature. This could also be due to the low channel aspect ratio. When using the silicone microchannel plate with cylindrical channels (aspect ratio of 1), the dimensionless droplet diameter was 6.5 ± 0.3. By increasing the channel aspect ratio from 1 to 1.9, the dimensionless droplet diameter therefore decreased significantly. Thus, the dimensionless droplet diameter would likely decrease if channels of the reported critical aspect ratio of 3.5 can be obtained.

The current beads are 2.9 ± 0.3 mm in diameter, much larger than the desired ~600 μm beads. A decrease in the dimensionless droplet diameter will decrease the bead diameter. However, even with a dimensionless droplet diameter of 2, the beads would still be 1.3 mm in diameter. The current channels are larger than the theoretical value to obtain 600 μm beads, with a hydraulic diameter approximately twice the necessary diameter. Producing the channels with a higher precision and better size control should allow the production of smaller alginate beads. The current alginate beads are slightly smaller than what would theoretically be produced from a nozzle with the same diameter as the channels. In the dripping regime, simple nozzle-based bead production would result in 3 mm diameter beads (Equation 1). While the current beads are approximately the same size, smaller microchannel emulsification produced beads could represent a significant improvement to the ratio of bead diameter to channel diameter.

The reported viscosity of 1.5 % Manugel® alginate solutions is of ~0.13 Pa·s [121]. Based on this viscosity, both the capillary number and microchannel dimension-modified capillary were calculated, as well as the buoyancy force and interfacial tension force (Table 4). The capillary number that corresponds to the operating parameters is significantly reduced by oblong channels compared to circular channels. This allows for higher flow rates or viscosity of the dispersed phase before the critical capillary number is reached and jetting occurs. Given that the aspect ratio of the channels is currently only 1.9, increasing this to the desired 3.5 will further decrease the capillary number and increase the possible production rates. The capillary number can also be decreased by increasing the contact angle of the dispersed phase on the microchannel surface. Surface modification of the plate could be used for this purpose. For example, the hydrophobic surface modification process described by Kobayashi *et al.* resulted in a water contact angle of 163^{o} [84].

Table 4. Forces and capillary numbers describing current microchannel emulsification system.

Capillary Number	Microchannel Dimension-Modified Capillary Number	Weber Number	Buoyancy Force (mN)	Interfacial Tension Force (mN)
2.15	1.13	7.3	0.08	0.02

6.0 Recommendations for future work

While uniform alginate beads can be produced using the current system, significant improvements could still be made. First, a flow chamber system with proper o-ring seals, similar to the one proposed in Figure 8, should be machined. The PTFE microchannel plate should also be laser micromilled with a higher precision to smooth the edges of the channel and achieve greater control over the channel size. This would allow microchannels with the proper dimensions and aspect ratio to be produced, which would aid in the reduction of bead size and size variability. Alternatively, a carbohydrate glass printer fitted with a rectangular nozzle could be used to produce the microchannel plate with a mould. The microchannel emulsification operating parameters should be systematically optimized using statistical design of experiments to reduce the size of the alginate beads to 600 μm. Some parameters that could be considered for the optimization include the flow rates, alginate concentration, surfactant type and concentration, temperature of the liquids, and channel length.

Once the desired size of beads has been produced, the physicochemical properties of the beads, including surface roughness, permeability, strength, and stability, should be characterized. It is important to determine the surface roughness of the alginate beads as it has implications for transplantation. High surface roughness can increase the host immune response after transplantation; thus, the surface roughness should be minimized [1]. Bead permeability also has important implications regarding host immune response post-transplantation. Bead with higher permeability towards antibodies increase the risk of graft rejection. The strength and stability of

the beads will play a role in determining the lifespan of the graft. Ideally, the beads would last for the lifetime of the patient. If the beads are prone to breaking or degrading over time, the blood glucose levels will no longer be regulated.

Pancreatic beta cell lines could be used as an initial cell model to determine the effect of the microchannel emulsification encapsulation process on mammalian cell survival and function. Beta cell survival and function after encapsulation by microchannel emulsification can be compared to cells encapsulated using the nozzle-based method or the stirred emulsification process. The effect of pH during acid oil exposure on cell survival and function should be investigated. Both the acid concentration in the continuous phase, as well as the residence time in the acidified continuous phase may affect cell survival, and should be kept at the minimum needed to ensure bead integrity. Once cell survival and function have been assessed using cell lines, islets could be encapsulated using microchannel emulsification.

7.0 Conclusions

Type 1 diabetes is an increasingly prevalent disease that has serious implications for diabetic patients and healthcare systems as a whole. Current insulin injection treatment methods are inadequate to properly maintain euglycemia and quality of life. Islet transplantation is a promising long-term therapeutic alternative to insulin injections. However, the requirement for chronic immune suppression post-transplantation limits the availability of this treatment for many patients. Encapsulation is a technique to immunoisolate the cells, creating a barrier between the graft and the host immune system. Islet microencapsulation in alginate beads is a common method investigated to avoid or reduce the need for immunosuppression after transplantation. Beads of approximately 600 μm in diameter allow for proper oxygen diffusion to the cells, while still ensuring that the cells are properly encapsulated. Traditional nozzle-based encapsulation methods

limit the viscosity of the alginate that can be used for encapsulation, resulting in beads that are permeable to antibodies unless further polymer coatings are applied. An alternative stirred emulsification encapsulation method can use much higher alginate viscosities, decreasing bead permeability, and also has high production rates and significant capacity for scalability. However, the beads produced using this method are very dispersed in size.

A need exists for a method to encapsulate cells in uniform, highly viscous alginate beads, at production rates relevant for clinical islet transplantation applications. The objective of this work was to develop microchannel emulsification for the production of uniform alginate beads. This work discusses the development of microchannel emulsification for this purpose. Specifically, this work shows that:

1) Microchannel emulsification can be used to produce uniform alginate beads at clinically relevant production rates.
2) Oblong channels that are preferentially wet by the continuous phase promoted droplet detachment.
3) Changing the alginate flow rate up to 4 mL/min/channel or alginate concentration between 0.5% - 2.5% alginate had little impact on the bead diameter obtained.

A dual-flow chamber system was designed to mount the microchannel plate between two flow channels. For continuous phases that are denser than alginate, the continuous phase flows through the top chamber, with a collection bath located above the chambers. Adding fetal bovine serum as a surfactant helped stabilize the emulsion. Modification of the continuous phase had a substantial effect on droplet formation, as it affected the forces promoting and counteracting droplet detachment. Novec 7500 engineering fluid, with a high density difference with alginate, proved most successful. The microchannel plate material and dimensions also played an important

role in droplet formation. The continuous phase must wet the surface of the microchannels, therefore a hydrophobic material should be used for the microchannel plate. Moreover, an increased channel aspect ratio increases droplet detachment. All of these parameters play a role in affecting the forces and parameters that influence droplet detachment.

The most successful microchannel emulsification process used a hydrophobic PTFE microchannel plate with a water contact angle of 109.2°. The channels had a hydraulic diameter of 639 μm and an aspect ratio of 1.9. Use of Novec 7500 Engineering Fluid as the continuous phase promoted droplet detachment due to the high density difference between the continuous phase and alginate. The alginate flow rate did not affect bead formation up to a critical flow rate, above which jetting occurred.

The current system allows the generation of 1.5% alginate beads at 4 mL/min/channel production rates. Therefore, the 100 mL required to treat one patient can be produced in just one minute with only 25 channels. Current production rates are higher than current microchannel emulsification production rates, and an improvement to the production rates using traditional nozzle based-devices, as seen in Table 1. Beads can readily be obtained via this process at alginate concentrations ranging between at least 0.5% to 1.5% alginate, at flow rates up to at least 4 mL/min/channel, without modification of the process parameters, contrary to most nozzle-based devices. Microchannel emulsification can be used to produce alginate beads that are highly uniform, with significantly decreased coefficients of variation from the stirred emulsification process. However, a drawback to both the stirred and microchannel emulsification system compared to traditional nozzle-based encapsulation techniques is that an extra step is required to separate the alginate beads from the organic phase prior to *in vitro* or *in vivo* use.

Microchannel emulsification has applications for the generation of emulsions in a variety of other industries, including the production of pharmaceutical, food, and household products. For example, water-in-oil emulsions are used in production of melt-resistant chocolate [122], flavour capsules for both food and pharmaceuticals [123], and pharmaceutical creams [124]. Microchannel emulsification represents a highly novel approach to cell encapsulation.

The development of a method to successfully produce uniform alginate beads for islet encapsulation represents a significant advancement towards islet transplantation therapy being widely available to type 1 diabetics without the need for chronic immune suppression. Islet transplantation can eliminate the need for frequent blood glucose monitoring and insulin injections. This work represents a step forward towards a therapy that can significantly improve the quality of life for patients living with type 1 diabetes.

8.0 References

1. de Vos, P., A.F. Hamel, and K. Tatarkiewicz, *Considerations for successful transplantation of encapsulated pancreatic islets.* Diabetologia, 2002. **45**(2): p. 159-173.
2. JDRF. *Type 1 Diabetes Facts*. 2016 [cited 2016 October 26]; Available from: http://www.jdrf.org/about/fact-sheets/type-1-diabetes-facts/.
3. JDRF. *Type 1 diabetes*. 2012 [cited 2016 October 26]; Available from: http://www.jdrf.org/about/fact-sheets/type-1-diabetes-facts/.
4. Group, T.D.C.a.C.T.R., *The effect of intensive treatment of diabetes on the development and progression of long-term complications in insulin-dependent diabetes mellitus. The Diabetes Control and Complications Trial Research Group.* The New England Journal of Medicine, 1993. **329**(14): p. 977-986.
5. Shapiro, A.M., et al., *Islet transplantation in seven patients with type 1 diabetes mellitus using a glucocorticoid-free immunosuppressive regimen.* N Engl J Med, 2000. **343**(4): p. 230-8.
6. Shapiro, A.M., et al., *International trial of the Edmontol Protocol for islet transplantation.* N Engl J Med, 2006. **355**(13): p. 1318-30.
7. Wang, N., et al., *Alginate encapsulation technology supports embryonic stem cells differentiation into insulin-producing cells.* Journal of Biotechnology, 2009. **144**(4): p. 304-312.
8. Hyder, A., C. Laue, and J. Schrezenmeir, *Effect of the immunosuppressive regime of Edmonton protocol on the long-term in vitro insulin secretion from islets of two different species and age categories.* Toxicol. in Vitro, 2005. **19**: p. 541-546.
9. Lim, F. and A.M. Sun, *Microencapsulated islets as bioartificial endocrine pancreas.* Science, 1980. **210**(4472): p. 908-10.
10. de Vos, P., et al., *Alginate-based microcapsules for immunoisolation of pancreatic islets.* Biomaterials, 2006. **27**: p. 5603-5617.
11. Gross, J.D., I. Constantinidis, and A. Sambanis, *Modeling of encapsulated cell systems.* J Theor Biol, 2007. **244**(3): p. 500-10.
12. De Vos, P., et al., *Association between capsule diameter, adequacy of encapsulation, and survival of microencapsulated rat islet allografts.* Transplantation, 1996. **62**(7): p. 893-9.
13. Serp, D., et al., *Characterization of an encapsulation device for the production of monodisperse alginate beads for cell immobilization.* Biotechnology and Bioengineering, 2000: p. 41-53.
14. Kulicke, W.M. and R. Kniewske, *The Shear Viscosity Dependence on Concentration, Molecular-Weight, and Shear Rate of Polystyrene Solutions.* Rheologica Acta, 1984. **23**(1): p. 75-83.
15. Li, R.H., D.H. Altreuter, and F.T. Gentile, *Transport characterization of hydrogel matrices for cell encapsulation.* Biotechnology and Bioengineering, 1996. **50**(4): p. 365-373.
16. Omer, *Survival and maturation of microencapsulated porcine neonatal pancreatic cell clusters transplanted into immunocompetent diabetic mice.*
17. Duvivier-Kali, V.F., et al., *Complete protection of islets against allorejection and autoimmunity by a simple barium-alginate membrane.* Diabetes, 2001. **50**(8): p. 1698-1705.

18. Rayat, G.R., et al., *Microencapsulation of neonatal porcine islets: protection from human antibody/complement-mediated cytolysis in vitro and long-term reversal of diabetes in nude mice.* Transplantation, 2000. **69**(6): p. 1084-90.
19. Korbutt, G.S., et al., *Improved survival of microencapsulated islets during in vitro culture and enhanced metabolic function following transplantation.* Diabetologia, 2004. **47**(10): p. 1810-8.
20. Dufrane, D., et al., *Six-Month Survival of Microencapsulated Pig Islets and Alginate Biocompatibility in Primates: Proof of Concept.* Transplantation, 2006. **81**(9): p. 1345-1353.
21. Sun, *Normalization of diabetes in spontaneously diabetic cynomologus monkeys by xenografts of microencapsulated porcine islets without immunosuppression.*
22. B.E., T., et al., *Safety and Viability of Microencapsulated Human Islets Transplanted Into Diabetic Humans.* Diabetes Care, 2009. **32**(10): p. 1887-1889.
23. Buder, B., et al., *Encapsulated islet transplantation: strategies and clinical trials.* Immune Network, 2013. **13**(6): p. 235-9.
24. Anderson, *Foreign body reaction to biomaterials.*
25. Schilfgaarde, v., *Factors influencing the properties and performance of.* 1999.
26. Avgoustiniatos, E.S. and C.K. Colton, *Effect of external oxygen mass transfer resistances on viability of immunoisolated tissue.* Annals of the New York Academy of Sciences, 2006. **831**(1): p. 145-167.
27. Macgregor, R.R., et al., *Small rat islets are superior to large islets in in vitro function and in transplantation outcomes.* American journal of physiology - Endocrinology and metabolism, 2006. **53**(5): p. E771-9.
28. Olsson, R. and P.O. Carlsson, *Oxygenation of cultured pancreatic islets.* Advances in Experimental Medicine and Biology, 2006. **578**: p. 263-8.
29. Fernandez, S.A., et al., *Emulsion-base islet encapsulation: predicting and overcoming islet hypoxia.* Bioencapsulation Research Group newsletter, 2014.
30. Shenkman, R.M., et al., *Effects of Energy Dissipation Rate on Islets of Langerhans: Implications for Isolation and Transplantation.* Biotechnology and Bioengineering, 2009. **103**(2): p. 413-423.
31. Hoesli, C., et al., *Pancreatic Cell Immobilization in Alginate Beads Produced by Emulsion and Internal Gelation.* Biotechnology and Bioengineering, 2011. **108**(2): p. 424-434.
32. de Vos, P. and e. al., *Polymers in cell encapsulation from an enveloped cell perspective.* Adv Drug Deliv Rev, 2014. **67-68**: p. 15-34.
33. Thus, B., et al., *The spatial distribution of calcium in alginate gel beads analysed by synchrotronradiation induced X-ray emission (SRIXE).* Carbohydr. Res., 1997. **297**: p. 01-105.
34. Steele, J.A.M., et al., *Therapeutic cell encapsulation techniques and applications in diabetes.* Advanced Drug Delivery Reviews, 2014: p. 74-83.
35. Prusse, U., et al., *Bead production with JetCutting and rotating disc/nozzle technologies.* Practical aspects of encapsulation technologies, 2002: p. 1-10.
36. Nedovi, V.A., et al., *Cell immobilisation by electrostatic droplet generation.* Landbauforschung Völkenrode, 2002. **241**: p. 11-17.
37. Rayleigh, L., *On the instability of jets.* Proc. London Math. Soc., 1878. **10**(1): p. 4-13.

38. Heinzen, C., A. Berger, and I. Marison, *Use of Vibration Technology for Jet Break-Up for Encapsulation of Cells and Liquids in Monodisperse Microcapsules.* Fundamentals of Cell Immobilisation Biotechnology, 2004. **8**: p. 257-275.
39. Champagne, C., et al., *A vortex- bowl disc atomizer system for the production of alginate beads in a 1500-liter fermenter.* Biotechnol Bioeng, 2000. **68**(6): p. 681-688.
40. Poncelet, D., et al., *Production of alginate beads by emulsification/internal gelation. 1. Methodology.* Appl. Microb. Biotechnol., 1992: p. 39-45.
41. Poncelet, D., et al., *Production of alginate beads by emulsion/internal gelation. II. Physiochemistry.* Appl. Microbiol. Biotechnol., 1995(43): p. 644-650.
42. Robitaille, R. and J.P. Halle, *Characterization and evaluation of the properties and functions of the microcapsules.* The bioartificial pancreas and other biohybrid techniques, Transworld Research Network, 2009: p. 67-85.
43. Hoesli, C., *Bioprocess development for the cell-based treatment of diabetes*, in *Chemical & Biological Engineering*. 2010, University of British Columbia: Vancouver.
44. Hoesli, C., et al., *Reversal of diabetes by BTC3 cells encapsulated in alginate beads generated by emulsion and internal gelation.* Society for Biomaterials, 2012. **100**(4): p. 1017-1028.
45. Cui, W., et al., *A membrane-mimetic barrier for islet encapsulation.* Transplant Proc, 2004. **36**(4): p. 1206-8.
46. Poncelet, D., et al., *A Parallel-Plate Electrostatic Droplet Generator - Parameters Affecting Microbead Size.* Applied Microbiology and Biotechnology, 1994. **42**(2-3): p. 251-255.
47. Senuma, Y., et al., *Alginate hydrogel microspheres and microcapsules prepared by spinning disk atomization.* Biotechnology and Bioengineering, 2000. **67**(5): p. 616-622.
48. Dufrane, D., et al., *Six-month survival of microencapsulated pig islets and alginate biocompatibility in primates: proof of concept.* Transplantation, 2006. **81**(9): p. 1345-53.
49. Koch, S., et al., *Alginate encapsulation of genetically engineered mammalian cells: comparison of production devices, methods and microcapsule characteristics.* J Microencapsul, 2003. **20**(3): p. 303-16.
50. Lewinska, D., et al., *Electrostatic microencapsulation of living cells.* Biocybernetics and Biomedical Engineering, 2008. **28**(2): p. 69-85.
51. Schwinger, C., et al., *High throughput encapsulation of murine fibroblasts in alginate using the JetCutter technology.* J Microencapsul, 2002. **19**(3): p. 273-80.
52. Nakashima, T., M. Shimizu, and M. Kukizaki, *Membrane Emulsification by Microporous Glass.* Key Engineering Materials, 1991. **61-62**: p. 513-516.
53. Kukizaki, M., *Shirasu porous glass (SPG) membrane emulsification in the absence of shear flow at the membrane surface: Influence of surfactant type and concentration, viscosities of dispersed and continuous phases, and transmembrane pressure.* MEMSCI Journal of Membrane Science, 2009. **327**(1): p. 234-243.
54. Dragosavac, M.M., et al., *Controlled production of oil-in-water emulsions containing unrefined pumpkin seed oil using stirred cell membrane emulsification.* MEMSCI Journal of Membrane Science, 2008. **322**(1): p. 178-188.
55. Shimoda, M., et al., *Swirl-Flow Membrane Emulsification for High Throughput of Dispersed Phase Flux through Shirasu Porous Glass (SPG) Membrane.* JOURNAL OF CHEMICAL ENGINEERING OF JAPAN, 2011. **44**(1): p. 1-6.
56. Williams, R., *Controlled dispersion using a spinning membrane reactor*. 2001.

57. Holdich, R.G., et al., *Membrane Emulsification with Oscillating and Stationary Membranes.* Ind. Eng. Chem. Res. Industrial & Engineering Chemistry Research, 2010. **49**(8): p. 3810-3817.
58. Vladisavljevic, G.T., et al., *Shirasu Porous Glass membrane emulsification: Characterisation of membrane structure by high-resolution X-ray microtomography and microscopic observation of droplet formation in real time.* MEMSCI Journal of Membrane Science, 2007. **302**(1): p. 243-253.
59. Vladisavljevic, G.T., S. Tesch, and H. Schubert, *Preparation of water-in-oil emulsions using microporous polypropylene hollow fibers: influence of some operating parameters on droplet size distribution.* CEP</cja:jid> Chemical Engineering & Processing: Process Intensification, 2002. **41**(3): p. 231-238.
60. Kobayashi, I., M. Nakajima, and S. Mukataka, *Preparation characteristics of oil-in-water emulsions using differently charged surfactants in straight-through microchannel emulsification.* Colloids and Surfaces A, 2003: p. 33-41.
61. Brans, G., et al., *Evaluation of microsieve membrane design.* MEMSCI Journal of Membrane Science, 2006. **278**(1): p. 344-348.
62. Van Rijn, C., et al., *Deflection and Maximum Load of Microfiltration Membrane Sieves Made with Silicon Micromachining.* JOURNAL OF MICROELECTROMECHANICAL SYSTEMS, 1997. **6**(1): p. 48-54.
63. Nazir, A., K. Schroen, and R. Boom, *High-throughput premix membrane emulsification using nickel sieves having straight-through pores.* J. Membr. Sci. Journal of Membrane Science, 2011. **383**(1-2): p. 116-123.
64. Vladisavljevic, G.T. and R.A. Williams, *Manufacture of large uniform droplets using rotating membrane emulsification.* YJCIS Journal of Colloid And Interface Science, 2006. **299**(1): p. 396-402.
65. Holdich, R.G., et al., *Continuous Membrane Emulsification with Pulsed (Oscillatory) Flow.* Ind. Eng. Chem. Res. Industrial & Engineering Chemistry Research, 2013. **52**(1): p. 507-515.
66. Dragosavac, M.M., et al., *Stirred cell membrane emulsification for multiple emulsions containing unrefined pumpkin seed oil with uniform droplet size.* J. Membr. Sci. Journal of Membrane Science, 2012. **392-393**: p. 122-129.
67. Vladisavljevic, G.T., I. Kobayashi, and M. Nakajima, *Production of uniform droplets using membrane, microchannel and microfluidic emulsification devices.* Microfluid Nanofluid Microfluidics and Nanofluidics, 2012. **13**(1): p. 151-178.
68. Jo, J., M.Y. Choi, and D.-S. Koh, *Size Distribution of Mouse Langerhans Islets.* Biophysical Journal, 2007. **93**(8): p. 2655-2666.
69. Whitesides, G.M., *The origins and the future of microfluidics.* Nature, 2006. **442**(7101): p. 368-73.
70. Xia, Y. and G.M. Whitesides, *Soft Lithography.* ANIE Angewandte Chemie International Edition, 1998. **37**(5): p. 550-575.
71. Morimoto, Y., W.H. Tan, and S. Takeuchi, *Three-dimensional axisymmetric flow-focusing device using stereolithography.* Biomedical microdevices, 2009. **11**(2): p. 369-77.
72. Wilson, M.E., et al., *Fabrication of circular microfluidic channels by combining mechanical micromilling and soft lithography.* Lab on a chip, 2011. **11**(8): p. 1550-5.

73. Dendukuri, D., et al., *Controlled synthesis of nonspherical microparticles using microfluidics.* Langmuir : the ACS journal of surfaces and colloids, 2005. **21**(6): p. 2113-6.
74. Zhao, C.-X. and A.P.J. Middelberg, *Two-phase microfluidic flows.* CES Chemical Engineering Science, 2011. **66**(7): p. 1394-1411.
75. De Menech, M., et al., *Transition from squeezing to dripping in a microfluidic T-shaped junction.* J. Fluid Mech. Journal of Fluid Mechanics, 2008. **595**: p. 141-161.
76. Xu, J., et al., *Correlations of droplet formation in T-junction microfluidic devices: from squeezing to dripping.* Microfluidics and Nanofluidics, 2008. **5**(6): p. 711-717.
77. Tan, Y.-C., V. Cristini, and A.P. Lee, *Monodispersed microfluidic droplet generation by shear focusing microfluidic device.* SNB Sensors & Actuators: B. Chemical, 2006. **114**(1): p. 350-356.
78. Steegmans, M.L., K.G. Schroën, and R.M. Boom, *Characterization of emulsification at flat microchannel Y junctions.* Langmuir : the ACS journal of surfaces and colloids, 2009. **25**(6): p. 3396-401.
79. Garstecki, P., H.A. Stone, and G.M. Whitesides, *Mechanism for Flow-Rate Controlled Breakup in Confined Geometries: A Route to Monodisperse Emulsions.* Physical Review Letters, 2005. **94**(16): p. 164501.
80. Yobas, L., et al., *High-performance flow-focusing geometry for spontaneous generation of monodispersed droplets.* Lab on a chip, 2006. **6**(8): p. 1073-9.
81. Foulds, I.G., D. Conchouso, and D. Castro, *Microfluidic device for high-volme production of monodisperse emulsions*. 2016, King Abdullah University of Science and Technology (Thuwal, SA) United States of America.
82. Kobayashi, I., et al., *Microchannel emulsification for mass production of uniform fine droplets: integration of microchannel arrays on a chip.* Microfluid Nanofluid, 2010: p. 255-262.
83. Kobayashi, I., et al., *Microscopic observation of emulsion droplet formation from a polycarbonate membrane.* Colloids and Surfaces A: Physiochemical and Engineering Aspects, 2002: p. 185-196.
84. Kobayashi, I., et al., *Production of monodisperse water-in-oil emulsions consisting of highly uniform droplets using asymmetric straight-through microchannel arrays.* Microfluid Nanofluid, 2009: p. 107-119.
85. Kobayashi, I., K. Uemura, and M. Nakajima, *Formulation of monodisperse emulsions using submicron channel arrays.* Colloids and Surfaces A Physiochemical and Engineering Aspects, 2009. **296**(1-3): p. 285-289.
86. Kobayashi, I., et al., *Generation of uniform drops via through hole arrays micromachined in stainless steel plates.* Microfluidics and Nanofluidics, 2008. **5**(5): p. 677-687.
87. Kawakatsu, T., G. Trägårdh, and C. Trägårdh, *Production of W/O/W emulsions and S/O/W pectin microcapsules by microchannel emulsification.* COLSUA</cja:jid> Colloids and Surfaces A: Physicochemical and Engineering Aspects, 2001. **189**(1): p. 257-264.
88. Sugiura, S., et al., *Preparation Characteristics of Monodispersed Water-in-Oil Emulsions Using Microchannel Emulsification.* JOURNAL OF CHEMICAL ENGINEERING OF JAPAN, 2001. **34**(6): p. 757-765.

89. Kobayashi, I., et al., *High-aspect-ratio through-hole array microfabricated in a PMMA plate for monodisperse emulsion production.* Microsyst Technol Microsystem Technologies : Micro- and NanosystemsInformation Storage and Processing Systems, 2008. **14**(9-11): p. 1349-1357.
90. Kawakatsu, T., Y. Kikuchi, and M. Nakajima, *Regular-sized cell creation in microchannel emulsification by visual micro-processing methods.* Journal of the American Oil Chemists' Society, 1997. **74**(3): p. 317-321.
91. Kawakatsu, T., et al., *Production of monodispersed oil-in-water emulsion using crossflow-type silicon microchannel plate.* Journal of Chemical Engineering of Japan, 1999: p. 241-244.
92. Kobayashi, I., et al., *Silicon array of elongated through-holes for monodisperse emulsions.* AIChE Journal, 2002. **48**(8): p. 1639-1644.
93. Vladisavijevic, G., I. Kobayashi, and M. Nakajima, *Effect of dispersed phase viscosity on maximum droplet generation frequency in microchannel emulsification using asymmetric straight-through channels.* Microfluidics and Nanofluidics, 2011. **10**(6): p. 1199-1209.
94. Kobayashi, I., et al., *Straight-through microchannel devices for generating monodisperse emulsion droplets several microns in size.* Microfluid Nanofluid, 2008: p. 167-177.
95. Kobayashi, I., S. Mukataka, and M. Nakajima, *Novel asymmetric through-hole array microfabricated on a silicon plate for formulating monodisperse emulsions.* Langmuir : the ACS journal of surfaces and colloids, 2005. **21**(17): p. 7629-32.
96. Sugiura, S., M. Nakajima, and M. Seki, *Effect of channel structure on microchannel emulsification.* Langmuir, 2002: p. 5708-5712.
97. Kobayashi, I., S. Mukataka, and M. Nakajima, *Effect of slot aspect ratio on droplet formation from silicon straight-through microchannels.* Journal of Colloid and Interface Science, 2004: p. 277-280.
98. Kobayashi, I., et al., *Silicon array of elongated through-holes for monodisperse emulsion droplets.* AIChE Journal, 2002. **48**(8): p. 1639-1644.
99. Kobayashi, I., S. Mukataka, and M. Nakajima, *CFD simulation and analysis of emulsion droplet formation from straight through microchannels.* Langmuir, 2004. **20**(22): p. 9868-77.
100. Kobayashi, I., K. Uemura, and M. Nakajima, *Effects of channel and operation parameters on emulsion production using oblong straight-through microchannels.* Japan Journal of Fooder Engineering, 2009. **10**(1): p. 69-75.
101. Kobayashi, I., et al., *CFD analysis of microchannel emulsification: Droplet generation process and size effect of asymmetric straight flow-through microchannels.* CES Chemical Engineering Science, 2011. **66**(22): p. 5556-5565.
102. Kobayashi, I., M. Nakajima, and S. Mukataka, *Preparation characteristics of oil-in-water emulsions using differently charged surfactants in straight-through microchannel emulsification.* Colloids Surf. A, 2003: p. 33-41.
103. Gu, H., M.H.G. Duits, and F. Mugele, *Droplets Formation and Merging in Two-Phase Flow Microfluidics.* International Journal of Molecular Sciences, 2011. **12**(4): p. 2572-2597.
104. Sugiura, S., et al., *Characterization of Spontaneous Transformation-Based Droplet Formation during Microchannel Emulsification.* J. Phys. Chem. B The Journal of Physical Chemistry B, 2002. **106**(36): p. 9405-9409.

105. van der Zwan, E., K. Schroën, and R. Boom, *A geometric model for the dynamics of microchannel emulsification.* Langmuir : the ACS journal of surfaces and colloids, 2009. **25**(13): p. 7320-7.
106. Butron Fujiu, K., et al., *Temperature effect on microchannel oil-in-water emulsification.* Microfluid Nanofluid Microfluidics and Nanofluidics, 2011. **10**(4): p. 773-783.
107. Frohn, A. and N. Roth, *Dynamics of droplets*. 2000, Berlin: Springer.
108. Kobayashi, I. and M. Nakajima, *Effect of emulsifiers on the preparation of food-grade oil-in-water emulsions using a straight-through extrusion filter.* Eur. J. Lipid Sci. Technol., 2002. **104**: p. 720-727.
109. Kobayashi, I., S. Mukataka, and M. Nakajima, *Effects of Type and Physical Properties of Oil Phase on Oil-in-Water Emulsion Droplet Formation in Straight-Through Microchannel Emulsification, Experimental and CFD Studies.* Langmuir, 2005. **21**(13): p. 5722-5730.
110. Miller, J.S., et al., *Rapid casting of patterned vascular networks for perfusable engineered three-dimensional tissues.* Nat Mater, 2012. **11**(9): p. 768-74.
111. Bégin-Drolet, A., et al., *Design of a novel 3D printer head for additive manufacturing of sugar glass for tissue engineering applications.* Submitted to: Additive Manufacturing, 2016.
112. Carpenter, A.E., et al., *CellProfiler: image analysis software for identifying and quantifying cell phenotypes.* Genome Biol, 2006. **7**(10): p. R100.
113. *3M™ Novec™ 7500 Engineered Fluid*. 2009; Available from: http://multimedia.3m.com/mws/media/65496O/3mtm-novectm-7500-engineered-fluid.pdf.
114. Chapman, T.M., *Biocompatible emulsifier*. 2000, Google Patents.
115. Khalid, N., et al., *Preparation of monodisperse aqueous microspheres containing high concentration of l-ascorbic acid by microchannel emulsification.* Journal of microencapsulation, 2015. **32**(6): p. 570-7.
116. Chuah, A.M., et al., *Preparation of uniformly sized alginate microspheres using the novel combined methods of microchannel emulsification and external gelation.* COLSUA Colloids and Surfaces A: Physicochemical and Engineering Aspects, 2009. **351**(1): p. 9-17.
117. Iwanaga, Y., et al., *Pancreas preservation for pancreas and islet transplantation.* Current opinion in organ transplantation, 2008. **13**(4): p. 445-451.
118. Maillard, E., et al., *Perfluorocarbons: new tool for islets preservation in vitro.* Transplantation proceedings, 2008. **40**(2): p. 372-4.
119. Enterprises, D. *Critical Surface Tension and Contact Angle with Water for Various Polymers*. 2016; Available from: https://www.accudynetest.com/polytable_03.html?sortby=contact_angle.
120. Prusse, U., et al., *Comparison of different technologies for alginate beads production.* Chemical Papers, 2008. **62**(4): p. 364-374.
121. Dalmoro, A., A.A. Barba, and M. dAmore, *Analysis of Size Correlations for Microdroplets Produced by Ultrasonic Atomization.* The Scientific World Journal The Scientific World Journal, 2013. **2013**(4): p. 1-7.
122. Killian, L.A. and J.N. Coupland, *Manufacture and Application of Water-in-Oil Emulsions to Induce the Aggregation of Sucrose Crystals in Oil: A Model for Melt-resistant Chocolate.* Food Biophysics, 2012. **7**(2): p. 124-131.

123. Garti, N. and D.J. McClements, *Encapsulation technologies and delivery systems for food ingredients and nutraceuticals*. 2012.
124. Kohri, N., et al., *Preparation of water in oil type cream with high content of water containing Kochia scoparia Fruit and Cnidium monnieri Fruit.* Yakugaku Zasshi Yakugaku Zasshi, 2011. **131**(12): p. 1835-1841.

Appendix 1. Troubleshooting

Problem	Typical Cause	Suggested Solution
Alginate beads are very large	The alginate has wet the surface of the microchannel plate around the exit of the microchannel	Wet the microchannel plate with continuous phase fluid prior to starting the emulsification. Ensure the continuous phase chamber is filled before allowing the alginate to pass through the microchannels.
Alginate is jetting	Alginate flow rate is too high	Lower alginate flow rate
Liquid in bottom chamber will not fill up to bottom of microchannel plate	Liquid has filled into top chamber before bottom chamber is fully filled	Ensure no liquid enters top chamber before bottom chamber is fully filled
Alginate beads have dents or flattened edges	Alginate beads are coming into contact with chamber walls before fully gelling, denting the beads	Increase the height of the continuous phase chamber
Alginate beads are coalescing into larger beads	Alginate beads are coming into contact with neighbouring beads before fully gelling	Increase space between microchannels, increase acid concentration, increase height of continuous phase chamber

Appendix 2. Standard Operating Procedure

SOP details

Title	Alginate bead production by microchannel emulsification
Description	This SOP describes how to produce uniform alginate beads by microchannel emulsification
Author	Karen Markwick
SOP number	043
Version number	1

	Name	Date	Signature
Prepared	Karen Markwick	29 October 2016	
Reviewed			
Reviewed			
Authorized			

Version changes

Version	Name	Date	Changes made
1	Karen Markwick	29 October 2016	First version

Table of contents

1 Purpose

This SOP describes how to produce alginate beads using microchannel emulsification.

2. Principle

Explain shortly the principle of the work instruction. It's a short background information for people unknown with the instruction.

3. Required materials

Workplace

This work should be conducted in a fully equipped laboratory. Preparation of the acidified continuous phase should be conducted in a fume hood.

Equipment

Microchannel emulsification flow chamber and collection bath
Microchannel plate
Tubing: L/S 13, 25, Tygon xx
30 and 60 mL syringes
Syringe pumps

Reagents

Name	Company	Location	Remarks/ Order no.
Alginate	FMC	R-7120, 4°C Fridge	
HEPES		R-7120, chemicals cabinet	
Sodium chloride		R-7120, chemicals cabinet	
Sodium hydroxide		R-7120, chemicals cabinet	
Calcium carbonate		R-7120, chemicals cabinet	
DMEM	Life Technologies	R-7120, 4°C Fridge	

FBS	VWR international CO.	R-7120, -20°C Freezer	40 mL aliquots available. Thaw overnight at 4°C. Opened aliquots can be kept up to 2 months at 4°C and combined with fresh aliquots if needed.
Penicillin/streptomycin (P/S)	Sigma-Aldrich	R-7120, -20°C Freezer	5 mL aliquots available. Opened aliquots can be kept up to 2 months at 4°C and combined with fresh aliquots if needed.
L-Glutamine	Life Technologies	R-7120, -20°C Freezer	5 mL aliquots available. Thaw at 37°C and vortex until completely dissolved. Opened aliquots can be kept up to 1 month at 4°C and combined with fresh aliquots if needed.
β-Mercaptoethanol	Sigma-Aldrich	R-7120, 4°C Fridge, -20°C Freezer	The 100X stock solution is aliquoted then placed in the -20°C Freezer
Acetic acid	Sigma-Aldrich	R-7120, flammables cabinet	
Novec 7500 Engineering Fluid	3M	R-7120, chemicals cabinet	

More information about safety and risk of chemicals can be found in the GROS-system (Registration of hazardous chemicals)

Preparation of working solutions

HEPES buffered saline solution:

10 mM HEPES
170 mM NaCl
pH 7.4

Medium:

500 mL DMEM
56.8 mL fetal bovine serum (FBS)
5.68 mL 200 mM L-glutamine
5.69 mL penicillin/streptomycin
2 µL ß-mercaptoethanol

4. Procedure

Working procedure

Preparation of dispersed and continuous phase:

1. Mix 29.7 mL of alginate, 1 mL of FBS, 2.3 mL of medium, and 1.65 mL of calcium carbonate solution.
2. Add 550 µL of acetic acid to 250 mL of Novec 7500 Engineered fluid.

Preparation of microchannel emulsification set-up:

1. Attach inlet and outlet tubing to both chambers using appropriate connectors.
2. Wet microchannels and surface of plate surrounding microchannels with continuous phase.
3. Place microchannel plate in between two chambers.
4. Using c-clamps, secure chambers with one clamp on the inlet side and two clamps on the outlet side.
5. Attach collection bath.

Production of alginate beads:

1. Fill 30 mL syringe with prepared alginate mixture. Attach syringe to inlet tubing of bottom chamber. Fill chamber until alginate touches the surface of the microchannel plate. Clamp the outlet tubing closed.
2. Fill 60 mL syringe with prepared Novec fluid. Attach syringe to inlet tubing of top chamber, and load syringe in pump. Pour the remaining prepared Novec fluid into the collection bath, and allow the fluid to fill the top chamber.
3. Manually push the alginate syringe with enough pressure until the alginate flows through the microchannels. Load the syringe into the pump.
4. Start the continuous phase pump at desired flow rate. Start the alginate pump at desired flow rate. Alginate will pass through microchannels, forming beads in the flowing continuous phase, and rise up into the collection bath.
5. If necessary, gently stir the contents of the collection bath to ensure the beads to not adhere to the walls of the collection bath before fully gelling.

Bead recovery:

1. Using a spatula, scoop the alginate beads from the collection bath into a 40 µm Nylon filter.
2. Wash the beads with medium until no colour change of the medium is observed.
3. The beads can then be stored in medium or used for analysis.

Take-down and cleaning of the flow chamber set-up:

1. Using a pipette, remove the contents of the collection bath. Disconnect the collection bath, and bring to washing.
2. Unscrew all c-clamps, holding the chambers together. Open the chambers and discard the contents in the appropriate waste collection. Bring the microchannel plate to washing.
3. Remove the alginate outlet clamp. Detach both inlet tubings from the respective syringes. Bring the flow chambers and tubing for washing.
4. Discard the syringes in appropriate waste collection.
5. Wash the microchannel plate immediately and allow to dry overnight before using again.
6. Detach all tubing and connectors from flow chambers. Soak overnight before washing. Allow to dry overnight before using again.

Safety

Handle acetic acid and preparation of continuous phase in fume hood. Handle all chemicals with care.

5. Waste

Ensure all liquid waste is disposed in the correct liquid waste container. Dispose of all solids in the biohazard waste.

6. References

SOP no	Title
007	Keeping a laboratory notebook